ANNUAL REVIEWS

*Annual Review of Marine Science*

# The Physical Oceanography of Ice-Covered Moons

Krista M. Soderlund,[1] Marc Rovira-Navarro,[2] Michael Le Bars,[3] Britney E. Schmidt,[4] and Theo Gerkema[5]

[1]Institute for Geophysics, Jackson School of Geosciences, University of Texas at Austin, Austin, Texas, USA; email: krista@ig.utexas.edu

[2]Lunar and Planetary Laboratory, University of Arizona, Tucson, Arizona, USA; email: mroviranavarro@arizona.edu

[3]CNRS, Aix Marseille Univ, Centrale Marseille, IRPHE, Marseille, France; email: lebars@irphe.univ-mrs.fr

[4]Departments of Astronomy and of Earth and Atmospheric Sciences, Cornell University, Ithaca, New York, USA; email: britneys@cornell.edu

[5]Department of Estuarine and Delta Systems, NIOZ Royal Netherlands Institute for Sea Research, Yerseke, The Netherlands; email: theo.gerkema@nioz.nl



Annu. Rev. Mar. Sci. 2024. 16:25–53

First published as a Review in Advance on September 5, 2023

The *Annual Review of Marine Science* is online at marine.annualreviews.org

https://doi.org/10.1146/annurev-marine-040323-101355



## Keywords

ocean worlds, physical oceanography, ocean dynamics, ice–ocean interactions

## Abstract

In the outer solar system, a growing number of giant planet satellites are now known to be abodes for global oceans hidden below an outer layer of ice. These planetary oceans are a natural laboratory for studying physical oceanographic processes in settings that challenge traditional assumptions made for Earth's oceans. While some driving mechanisms are common to both systems, such as buoyancy-driven flows and tides, others, such as libration, precession, and electromagnetic pumping, are likely more significant for moons in orbit around a host planet. Here, we review these mechanisms and how they may operate across the solar system, including their implications for ice–ocean interactions. Future studies should continue to advance our understanding of each of these processes as well as how they may act together in concert. This interplay also has strong implications for habitability as well as testing oceanic hypotheses with future missions.

## 1. INTRODUCTION

For centuries, the subject of physical oceanography was limited to Earth's oceans and seas. The discovery of oceans buried beneath the icy crusts of moons in the outer solar system has widened the horizons beyond Earth. In the last decades, observations and process-based studies have started to unveil the complex and diverse dynamics possible in these distant oceans. Yet many questions remain in this new era of planetary oceanography. The aim of this article is to review our current understanding of the dynamics of ice-covered oceans and underline the main outstanding questions.

To study ocean dynamics, it is necessary to know their physical characteristics and understand their geophysical context. Data about extraterrestrial oceans, however, are scarce. For some moons, observations have provided unambiguous evidence of the existence of subsurface oceans (Europa, Ganymede, Enceladus, and Titan); for others, observations or theoretical models either suggest or allow for possible oceans (**Figure 1**). Our knowledge of the characteristics of such oceans is limited (at best) to constraints on ocean thickness and composition, which affects efforts to understand planetary ocean dynamics. Section 2 provides a concise overview of the characteristics of

Supplemental Material >

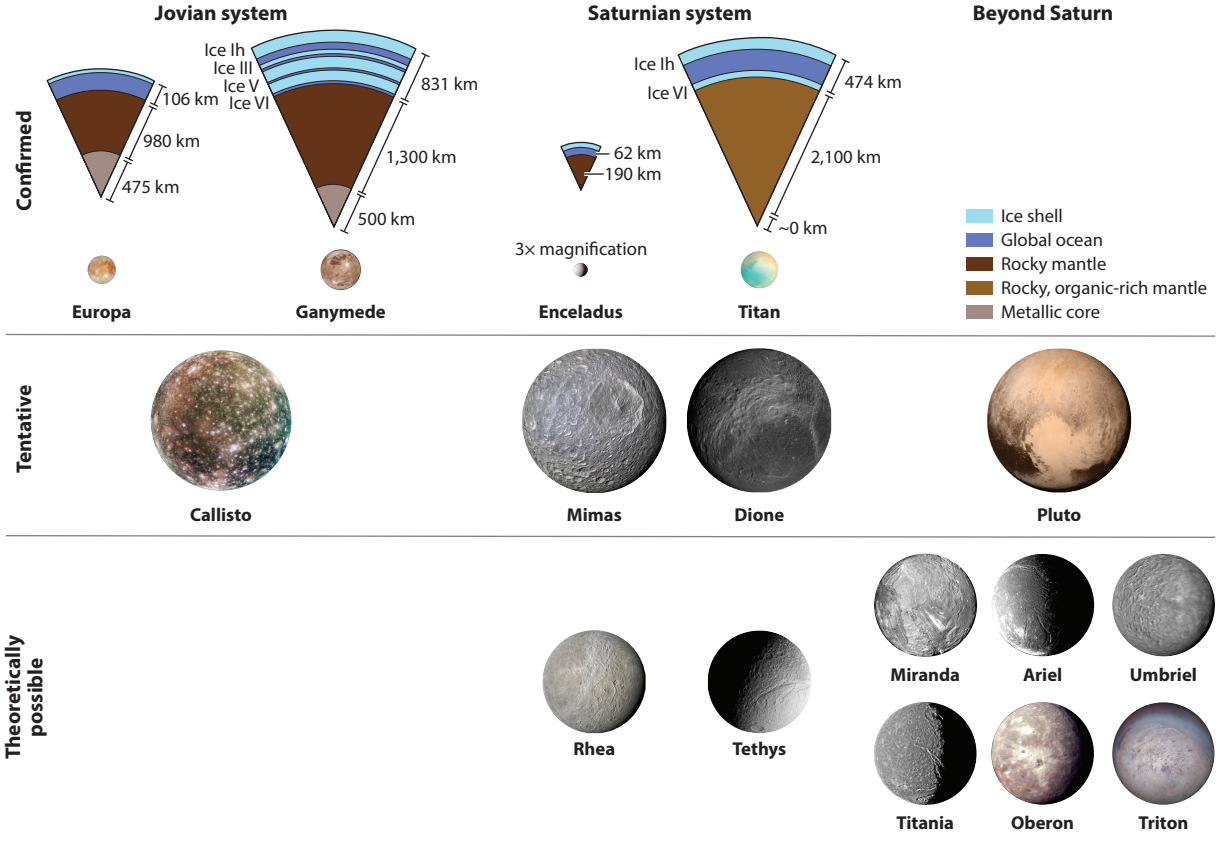


**Figure 1**

Confirmed, tentative, and theoretical ocean worlds in the outer solar system (not to scale). Additional information about the moons can be found in **Supplemental Tables 1 and 2**. Internal structure models for confirmed ocean worlds adapted with permission from Vance et al. (2018).

ocean-bearing moons and their interiors; Nimmo & Pappalardo (2016) published an in-depth review on the topic.

Beyond the physical characteristics of ice-covered oceans, we can infer their dynamics using computational and analytical models, laboratory experiments, and Earth analogs (both the oceans and the core). However, laboratory experiments are limited by scale, Earth analogs by sometimes stark differences between Earth's ocean and those of icy ocean worlds, and numerical ocean models by existing computational resources. This last limitation makes it impossible to directly solve the equations governing ocean dynamics. Instead, different assumptions are employed to simplify the system and study specific processes. In Section 3, we review the equations governing ocean dynamics and the simplifying approximations often used.

Different processes can result in ocean currents. We distinguish among flows that are buoyancy driven (Section 4), mechanically driven (Section 5), and electromagnetically driven (Section 6). Buoyancy-driven flows are caused by the exchange of heat and salt between the ocean and the underlying mantle/core and overlying ice shell. The decay of radioactive material and tidal heating within the mantle result in a basal heat flux. Salts and other impurities may be introduced by water–rock reactions below the seafloor, while melting and/or freezing of the overlying ice shell will freshen or introduce salts locally. These processes alter the density of the ocean and drive ocean circulation. Mechanically driven flows are the consequence of the moons' orbits and rotation. Icy moons experience gravitational tides that deform them and stir their oceans. Tidal torques also cause periodic changes in the rotation of the moons (e.g., libration and precession) that can drive ocean currents. Finally, electromagnetic interactions with their host planet's magnetic field are an additional mechanism for ocean currents. We finish by providing perspectives from Earth (Section 7), summarizing the key points, and highlighting future issues for the field.

## 2. ICE-COVERED OCEAN WORLDS

### 2.1. The Jovian System

The *Voyager* and *Galileo* missions revealed that the Jovian moons exhibit a gradient in geological activity. Io, the rocky innermost moon, is the most volcanically active world in the Solar System and is devoid of impact craters; Europa's icy surface has few craters, exhibits global resurfacing, and is tectonized; Ganymede presents heavily cratered plains interrupted by bright, less cratered younger terrain textured by ridges and troughs; and Callisto is heavily cratered and shows little evidence of geological activity (e.g., Schenk 2010). The gradient in geological activity is linked to the moons' orbits. The three innermost Galilean moons participate in a Laplace resonance (Peale 1999). The moons mutually exert a coherent, periodic perturbation to each other that forces their orbital eccentricity. The nonzero eccentricity results in tidal forces, and dissipation converts part of the tidal energy into internal heat, a process known as tidal heating. Io experiences the highest amount of tidal heating, followed by Europa; Ganymede and Callisto are not experiencing significant tidal heating at present, but Ganymede might have in the past (Bland et al. 2009, Downey et al. 2020).

The density of the Galilean moons decreases with distance away from Jupiter; the water/rock mass ratio changes from ∼5% for Europa to ∼50% for Callisto (see Soderlund et al. 2020 and references therein). Geodetic measurements by the *Galileo* mission indicated that Europa has an 80–170-km-thick $H_2O$ layer above a rocky mantle that could be either enriched in metals or fully differentiated into a silicate envelope and a metallic core, with the second scenario favored. Ganymede is differentiated into a core with a radius of ∼500–1,000 km, surrounded by a silicate mantle and an ∼800-km-thick $H_2O$ layer. Callisto may not be fully differentiated; gravity data are consistent with both two-layered models consisting of a metal–rock–ice core beneath an

~350-km hydrosphere and three-layered models where the metallic elements have separated from the silicates.

The small density contrast between liquid water and ice precluded deducing the state of the hydrosphere from gravity data alone. The detection of induced magnetic fields around the moons by *Galileo* demonstrated the presence of an electrically conductive layer—i.e., a salty ocean—beneath the surfaces of Europa (Kivelson et al. 2000), Ganymede (Kivelson et al. 2002), and Callisto (Khurana et al. 1998). A Europan subsurface ocean is also consistent with its surface geology (e.g., Pappalardo et al. 1999). The case of a subsurface ocean in Ganymede is further supported by Hubble Space Telescope aurora observations (Saur et al. 2015); for Callisto, however, the magnetic signal may also be caused by its ionosphere (Hartkorn & Saur 2017). Europa's subsurface ocean is in direct contact with the silicate shell. In contrast, the high pressures attained within Ganymede's hydrosphere result in the formation of high-pressure ices (Journaux et al. 2020).

Ocean thickness and electrical conductivity cannot be inferred independently from existing magnetic data, and the dominant salts and salinities of subsurface oceans are poorly constrained (for a review, see Soderlund et al. 2020). For Europa, the preponderance of geological evidence suggests ice shells in the tens of kilometers (e.g., Pappalardo et al. 1999), though other estimates range from a few kilometers (Walker & Rhoden 2022) to more than ~50 km (Vilella et al. 2020). In the absence of significant tidal heating at present, the outer shells of Ganymede and Callisto are likely thicker. The feedback between interior and orbital dynamics likely drives temporal variations of shell thickness over geological timescales (e.g., Hussmann & Spohn 2004) and potentially spatial variations as well (e.g., Ojakangas & Stevenson 1989).

## 2.2. The Saturnian System

Titan represents ~95% of the mass of Saturn's moons, with the remaining mass in a collection of smaller icy satellites. How this system architecture formed is still debated and has important implications for the moon ages (e.g., Sasaki et al. 2010, Ćuk et al. 2016). The *Cassini–Huygens* mission provided constraints on the interior structure of Titan and characterized its methane-based hydrological cycle (for a review, see Sotin et al. 2021). The density and moment of inertia indicate that Titan has an ~400-km-thick $H_2O$ layer above a core with a density of ~2,500 kg $m^{-3}$. Measurements of Titan's tidal response and obliquity indicate that it has an ocean with a density higher than 1,100 kg $m^{-3}$ and as high as 1,350 kg $m^{-3}$. The lower end can be met by pure water with 3 wt% ammonia; higher densities could be explained by the presence of ammonium sulfate, magnesium sulfate, or chlorides. Shape and gravity data indicate an ice-shell thickness in the range of 40–100 km, with potential variations in thickness or density. Shell thickness variations could be caused by nonuniform heating and could be as high as ~12 km, while density variations could be driven by Titan's methane cycle. Thickness variations are suggestive of a cold conductive shell, consistent with the limited tidal heating required to sustain the moon's relatively high free (i.e., not forced via a resonance) orbital eccentricity. These variations may suggest that oceanic heat flux into the ice shell peaks at high latitudes, with a minimum near the equator (Kvorka et al. 2018).

Saturn's midsized moons are compositionally similar, with varied geology (e.g., Castillo-Rogez et al. 2018). Mimas and Rhea show no sign of recent activity, and Tethys and Dione have evidence for past resurfacing, while Enceladus features a somewhat two-faced surface, with tectonized young regions and older cratered plains. Despite being just 252 km in radius (compared with 2,574 km for Titan and 1,563 km for Europa), Enceladus is highly active, with plumes of water venting hundreds of kilometers above its south polar limb (Porco et al. 2006). *Cassini* showed that Enceladus possesses a porous, low-density core ($\rho \sim 2{,}300$ kg $m^{-3}$) below a global ocean and an

ice shell (for a review, see Hemingway et al. 2018). Shape and gravity modeling suggest that heat flux at the top of the ocean is characterized by strong degree 2 and 3 zonal components (Čadek et al. 2019). The detection of salt grains, silicate particles, $H_2$, and $N_2$ in the material ejected by the plumes indicates that the subsurface ocean is in contact with the core and has ongoing hydrothermal activity (Hsu et al. 2015, Waite et al. 2017). Shape and gravity data are compatible with a subsurface ocean in Dione beneath an ~60–140-km-thick shell (Zannoni et al. 2020). The librations of Mimas indicate that it might have a subsurface ocean (e.g., Rhoden & Walker 2022), which contrasts with its inactive surface and high free eccentricity. The formation and longevity of the oceans of Saturn's midsized moons depend on their orbital evolution, which is still poorly understood (e.g., Neveu & Rhoden 2019).

## 2.3. Beyond Saturn

Without the benefit of dedicated missions to the Uranian and Neptunian systems, our knowledge of the moons in these systems derives mainly from data returned by the *Voyager 2* mission (e.g., Smith et al. 1986, 1989). The Uranian moons have densities similar to those of Saturn's midsized moons. Miranda and Ariel experienced resurfacing events as recently as 100 Ma and heat fluxes (~10–100 mW $m^{-2}$) higher than those presently experienced by Europa and Enceladus (Beddingfield et al. 2015, Peterson et al. 2015). While none of the moons are in an orbital resonance at present, they have gone through different resonances in the past (e.g., Ćuk et al. 2020). These resonances likely caused the resurfacing events and high heat fluxes recorded on Miranda's and Ariel's surfaces and might have resulted in the formation of subsurface oceans. Subsurface oceans are also possible in Titania and Oberon from radiogenic heating alone (Bierson & Nimmo 2022). Ammonia has been detected in Miranda and Ariel (Bauer et al. 2002, Cartwright et al. 2020), which may have helped preserve these oceans until the present (cf. Castillo-Rogez et al. 2023).

Neptune's moon Triton differs from other icy satellites in that it is a captured Kuiper Belt object in a retrograde orbit tilted with respect to the ecliptic (e.g., McKinnon 1984). Triton has a young surface with extensive resurfacing (e.g., Smith et al. 1989) and plumes that might be driven by a solid-state greenhouse effect or internal heating (e.g., Hofgartner et al. 2022). Triton likely experienced strong tides during its capture that melted its interior (Ross & Schubert 1990), which could have been maintained by a combination of radiogenic and tidal heating until the present (e.g., Nimmo & Spencer 2015).

## 2.4. Earth from Afar

In modeling ice-covered ocean worlds, we are thus in a data-poor, possibility-rich universe. Modeling the oceans of these worlds is akin to modeling Earth's oceans without detailed knowledge of ocean salinity, structure, or bathymetry; a modeler could do little more than assume an unstratified or uniformly stratified ocean of nearly uniform depth. As terrestrials, we know how disparate these idealized assumptions are from what our real ocean looks like. It is illuminating to reflect on how this complex reality affects our ocean's dynamics and to tentatively explore which of these factors may be at work in ice-covered ocean worlds.

By way of example, **Figure 2** shows a meridional transect from the Pacific Ocean. The bathymetry is uneven, exhibiting ridges and seamounts throughout, as well as a deep trench. The effect of bathymetry on ocean dynamics is wide-ranging. For example, continental slopes act as a wave guide for tides and shape the pattern of tides, including their resonance characteristics. Internal tides reflecting from a slope can result in intensification of internal tidal beams, making ridges and seamounts hotspots of internal tide breaking and shear instabilities, and hence of mixing. Abyssal mixing plays a key role in maintenance of the large-scale meridional overturning

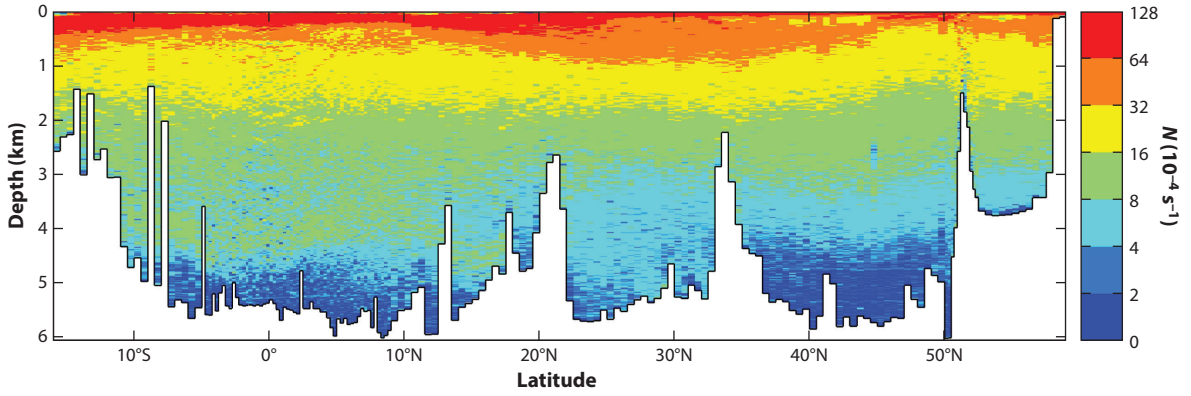


**Figure 2**

Buoyancy frequency $N$ along a transect in the Pacific Ocean (for the definition of $N$, see Equation 3 in the main text). This transect follows the meridian at longitude 179°E, except for an eastward bend in the Bering Sea. Notice that the color scale is logarithmic. Data are from the World Ocean Circulation Experiment (WOCE) Hydrographic Programme. Figure adapted from Gerkema (2019).

circulation (Wunsch & Ferrari 2004). Below the surface, both ice and seafloor topography might act as internal wave generators, and might trigger significant material and heat exchange. However, our ability to study these processes is hindered by our limited knowledge of such roughness.

Another conspicuous feature in **Figure 2** is the ocean's nonuniform stratification ($N$) and horizontally layered structure. The top layer is shaped by solar radiation, and atmosphere–ocean interactions create an upper mixed layer in the upper 50 m or so (barely discernible in the figure). Beneath this thin layer, temperature undergoes a rapid change with depth in tropical regions and at midlatitudes in summer. This layer of high $N$ is called the thermocline or pycnocline and occupies the upper few hundred meters. The deeper part of the ocean, beneath 1 km, always has temperatures lower than 5°C, even in the tropics. For moons of the outer planets, the structure of $N$ is likely to be very different from that in **Figure 2**, and might instead resemble more exotic Earth environments in the polar regions, where the stratifying component shifts from temperature to salinity (e.g., Vance & Goodman 2009, Soderlund et al. 2020, Lawrence 2022).

## 3. GOVERNING EQUATIONS AND COMMON APPROXIMATIONS

Supplemental Material >

The equations governing ocean dynamics are the mass, momentum, and salinity conservation equations; the heat equation; an equation of state; Poisson's equation; the induction equation; and the no-magnetic-monopole requirement (Equations 1a–h below, respectively). The full equations are given in the **Supplemental Appendix**; below, we simplify using the anelastic approximation (which filters sound waves from the equations of motion) and assume a linear equation of state. The density $\rho$, pressure $p$, temperature $T$, potential temperature $\theta$, and salinity $S$ are written in terms of a known background assumed to be adiabatic, isohaline, and hydrostatic (denoted by a 0 subscript) and a perturbation (denoted by primes). The governing equations are then as follows (Ingersoll 2005):

$$\nabla \cdot (\rho_0 \mathbf{u}) = 0, \tag{1a}$$

$$\frac{\mathrm{D}\mathbf{u}}{\mathrm{D}t} + 2\boldsymbol{\Omega} \times \mathbf{u} = -\frac{1}{\rho_0}\nabla p' + \frac{\rho'}{\rho_0}\mathbf{g} - \nabla\phi' + \nu\nabla^2\mathbf{u} + \frac{1}{\mu_0\rho_0}(\nabla \times \mathbf{B}) \times \mathbf{B} - \frac{\mathrm{d}\boldsymbol{\Omega}}{\mathrm{d}t} \times \mathbf{r}, \tag{1b}$$

$$\frac{\mathrm{D}S'}{\mathrm{D}t} = Q_1, \tag{1c}$$

$$\frac{\mathrm{D}\theta'}{\mathrm{D}t} = \frac{\theta_0}{T_0}\frac{Q_2}{c_\mathrm{p}}, \tag{1d.}$$

$$\rho' = \rho_0\left(-\alpha\theta' + \beta S' + \frac{1}{\rho_0 c_\mathrm{s}^2}p'\right), \tag{1e.}$$

$$\nabla^2\phi' = 4\pi\mathcal{G}\rho', \tag{1f.}$$

$$\frac{\partial \mathbf{B}}{\partial t} = \nabla\times(\mathbf{u}\times\mathbf{B}) - \nabla\times\left(\frac{1}{\mu_0\sigma}\nabla\times\mathbf{B}\right), \tag{1g.}$$

$$\nabla\cdot\mathbf{B} = 0. \tag{1h.}$$

Here, $\mathbf{u}$ is the velocity field, $\mathbf{g}$ is the gravitational acceleration, $\phi = \phi_0 + \phi'$ is the gravitational potential with both static and perturbation components, $\mathcal{G}$ is the gravitational constant, $\mathbf{B}$ is the magnetic field, $\boldsymbol{\Omega}$ is the rotation rate of the reference frame of the moon, $\mathrm{D}/\mathrm{D}t$ is the material derivative, $\mathbf{r}$ is the position vector, $\nu$ is the kinematic viscosity, $\alpha$ is the thermal expansion coefficient, $\beta$ is the saline contraction coefficient, $c_\mathrm{p}$ is the specific heat capacity, $c_\mathrm{s}$ is the speed of sound, $\sigma$ is the electrical conductivity, and $\mu_0$ is the vacuum magnetic permeability. $Q_1$ represents sinks and sources of salinity, and $Q_2$ represents sinks and sources of heat, including irreversible (diffusive) processes (see the **Supplemental Appendix**). The domain, initial, and boundary conditions must also be specified; the boundary conditions couple the dynamics of the ocean to the ice shell and deep interior.

Supplemental Material >

**Table 1** lists commonly used approximations, such as the anelastic (ii) and Boussinesq (iii) approximations. Nearly all planetary oceanography studies neglect magnetic fields (i), eliminating Equations 1g and 1h and the Lorentz force from Equation 1b (cf. Tyler 2011a,

**Table 1 Common approximations**

| ID | Approximation | Typically used if. . . | Filtered/ignored phenomena |
|---|---|---|---|
| i | No magnetism | Electrically insulating | Magnetic induction, Lorentz force |
| ii | Anelastic approximation | $\omega L \ll c_\mathrm{s}$ | Sound waves |
| iii | Boussinesq approximation | ii, $\rho_0$ is constant | No density variations beyond buoyancy |
| iv | Linear equation of state | $\alpha$, $\beta$ are constant | Cabbeling, thermobaricity |
| v | Isohaline | $Q_1 \approx 0$ | Variations in salinity |
| vi | Isentropic | $Q_2 \approx 0$ | Non-adiabatic, nonreversible processes |
| vii | Thin-layer approximation | $H \ll R$ | Radial gravity variations |
| viii | Spherical-body approximation | $\varepsilon \ll 1$ | Horizontal gravity component |
| ix | Massless approximation | $\phi^{(\mathrm{SG})} \ll \phi_0$ | Self-gravity |
| x | Rigid mantle/core | $\eta_\mathrm{b} \ll 1$ | No ocean bottom displacements |
| xi | Constant rotational rate | $\Omega = \Omega_0$ | Poincaré force, spin-driven flows |
| xii | Linearization | Waves have small amplitudes | Turbulence, wave breaking |
| xiii | Traditional approximation | $H/L \ll 1$ | Horizontal rotation vector component |
| xiv | Shallow-water approximation | $H/L \ll 1$ | Internal inertial waves |
| xv | Unstratified ocean | $N \approx 0$ | Internal gravity waves |
| xvi | Nonrotating body | $\Omega/\omega \ll 1$ | Rossby waves |
| xvii | Ocean in equilibrium | xv, xvi, $\omega L \ll c_\mathrm{surf}$ | All types of ocean waves |

$c_\mathrm{s}$ and $c_\mathrm{surf}$ are the sound and surface wave speed, respectively. $\varepsilon$, $\Omega$, and $R$ are the body's oblateness, rotational frequency, and radius, respectively. $H$ and $N$ are the ocean's thickness and buoyancy frequency, respectively. $\eta_\mathrm{b}$ is the displacement of the ocean bottom due to mechanical forces, and $\phi^{(\mathrm{SG})}$ is the gravitational potential arising from the body's self-gravitation. $L$ and $\omega$ are the characteristic wavelength and frequency of the problem, respectively; for tides, they correspond to the body's radius $R$ and the tidal frequency.

Gissinger & Petitdemange 2019, Vance et al. 2020). Additionally, in some studies, the thin-layer (vii) and spherical-body (viii) approximations are utilized, where both gravity and the centrifugal acceleration are assumed to be constant throughout the water column and its nonradial components are ignored (see Section 5).

Buoyancy-driven and mechanically driven flows are often studied separately. Convective motions are the consequence of diabatic processes (here loosely understood as exchange of heat and salinity) and determine the stratification structure of the ocean. In contrast, to study mechanically driven flows, diabatic processes are neglected and the stratification structure is taken as a given. It must be noted, however, that the two are closely linked. Mixing and dissipation due to mechanically driven flows play a key role in the thermal (and haline) structure of the ocean. Moreover, studying the coupling between the ocean and the ice shell and the exchange between the two requires understanding both simultaneously.

For buoyancy-driven flows, the criterion for convective instability requires the superadiabaticity of the fluid to exceed any compositional gradients: $\nabla_{\mathrm{T}} - \nabla_{\mathrm{ad}} > (\beta/\alpha)\nabla_{\mathrm{S}}$, known as the Ledoux instability criterion. Here, $\nabla_{\mathrm{T}}$, $\nabla_{\mathrm{ad}}$, and $\nabla_{\mathrm{S}}$ are the radial temperature, adiabatic temperature, and salinity gradients, respectively. In the absence of compositional gradients, the Ledoux instability criterion simplifies to the Schwarzschild criterion: $\nabla_{\mathrm{T}} - \nabla_{\mathrm{ad}} > 0$. For these flows generally, the perturbing potential is ignored and the ocean geometry is assumed to be fixed (ix, x), the rotational rate is assumed to be constant (xi), and $Q_2$ is assumed to consist of thermal diffusion only; other sources and sinks of heat (e.g., viscous and ohmic heating) are ignored but can still be present via the boundary conditions. $Q_1$ is kept as a generic sink/source of salinity, hence the difference in form compared with the heat equation. Furthermore, the Boussinesq approximation (iii) is often used instead of the anelastic approximation (ii). Here, the background density and potential temperature are assumed to be constant and the density perturbation to be independent of pressure perturbations (for a detailed discussion, see the chapter 14 appendix in Tritton 1998). These assumptions reduce the nonmagnetic (i) Equation 1 to

$$\nabla \cdot \mathbf{u} = 0, \tag{2a.}$$

$$\frac{\mathrm{D}\mathbf{u}}{\mathrm{D}t} + 2\boldsymbol{\Omega_0} \times \mathbf{u} = -\frac{1}{\rho_0}\nabla p' - \alpha T'\mathbf{g} + \beta S'\mathbf{g} + \nu\nabla^2\mathbf{u}, \tag{2b.}$$

$$\frac{\partial S'}{\partial t} + (\mathbf{u} \cdot \nabla)S' = Q_1, \tag{2c.}$$

$$\frac{\partial T'}{\partial t} + (\mathbf{u} \cdot \nabla)T' = \kappa\nabla^2 T', \tag{2d.}$$

with thermal diffusivity $\kappa = k/c_{\mathrm{p}}\rho$ and thermal conductivity $k$.

For mechanically driven flows, it is normally assumed that processes are isohaline (v) and isentropic (vi). Making these assumptions and neglecting small terms reduces the nonmagnetic (i) Equation 1 to (Gerkema & Zimmerman 2008)

$$\nabla \cdot \mathbf{u} = 0, \tag{3a.}$$

$$\frac{\mathrm{D}\mathbf{u}}{\mathrm{D}t} + 2\boldsymbol{\Omega} \times \mathbf{u} = -\frac{1}{\rho_0}\nabla p' + \frac{\rho'}{\rho_0}\mathbf{g} - \nabla\phi' + \nu\nabla^2\mathbf{u} - \frac{\mathrm{d}\boldsymbol{\Omega}}{\mathrm{d}t} \times \mathbf{r}, \tag{3b.}$$

$$\frac{g}{\rho_0}\frac{\mathrm{D}\rho'}{\mathrm{D}t} - N^2 u_{\mathrm{r}} = 0, \tag{3c.}$$

$$\nabla^2\phi' = 4\pi\mathcal{G}\rho', \tag{3d.}$$

where $u_r$ is the radial velocity and $N^2 = -(g/\rho_0)(\mathrm{d}\rho_0/\mathrm{d}r + \rho_0 g/c_s^2)$ is the square of the buoyancy frequency.

**LTEs:** Laplace tidal equations

Equation 3 still contains rich and complex dynamics. The equations are often linearized (xii) to study ocean waves, which removes different phenomena that can cause turbulence. The traditional approximation (xiii) and shallow-water approximation (xiv) are also often employed. The traditional approximation consists of neglecting the terms of the Coriolis force that arise from the nonradial component of the rotation vector to separate vertical and horizontal dynamics. In the shallow-water approximation, the inertial term in the radial momentum equation is ignored, transforming it into a force balance between the pressure gradient and the gravitational and Coriolis accelerations, or, when used in combination with the traditional approximation (xiii), simply into hydrostatic balance. The traditional and shallow-water approximations are typically invoked when the horizontal length scale of ocean motions is much larger than the ocean thickness; however, their validity involves more subtle aspects (e.g., Gerkema et al. 2008). If the ocean is unstratified (xv), these assumptions lead to the classic Laplace tidal equations (LTEs):

$$\partial_t(\eta_s - \eta_b) + \nabla \cdot (H\bar{\mathbf{u}}) = 0, \tag{4a}$$

$$\partial_t \bar{\mathbf{u}} - f\bar{\mathbf{u}} \times \boldsymbol{e}_r = -\frac{1}{\rho_0}\nabla p' - \nabla\phi' + D(H, \bar{\mathbf{u}}), \tag{4b}$$

$$p' = g\rho_0\eta_s + q, \tag{4c}$$

where $\eta_s$ and $\eta_b$ are radial displacements of the ocean surface and bottom, respectively; $\bar{\mathbf{u}}$ is the average horizontal velocity; $f = 2\Omega\cos\theta_c$ is the Coriolis parameter, with $\theta_c$ being colatitude; and $q$ is the pressure exerted by the ice shell. $D(H, \bar{\mathbf{u}})$ parameterizes dissipation within the system, and the form of this function is uncertain. For Earth, $D(H, \bar{\mathbf{u}})$ can be tuned to fit a large set of observations (e.g., Green & Nycander 2013). For icy moons, we do not have the benefit of such observations. In analogy with Earth, it can be assumed that energy is dissipated at the ocean boundaries due to bottom drag, $D = c_D|\bar{\mathbf{u}}|\bar{\mathbf{u}}/H$, with $H$ the ocean thickness and $c_D$ the bottom drag coefficient (e.g., Hay & Matsuyama 2017). However, the dissipation mechanisms at play in subsurface oceans might be different from those in Earth's oceans. Because of this, many studies have considered simpler linear dissipation terms such as $\alpha_R\bar{\mathbf{u}}$, with $\alpha_R$ being the Rayleigh coefficient (e.g., Tyler 2011b), or $\nu_{turb}\Delta\bar{\mathbf{u}}$, with $\nu_{turb}$ being the horizontal eddy viscosity (Chen et al. 2014), and varied the dissipation parameters over orders of magnitude.

If the forcing frequency ($\omega$) is much higher than the rotational frequency of the body ($\Omega$), the rotation of the moon can be neglected (xvi). Finally, if the surface gravity wave speed is much larger than the speed at which the perturbation propagates, mechanically driven ocean dynamics can be ignored altogether, and the ocean follows the equilibrium tide (xvii), given by $p'/\rho_0 + \phi' = 0$.

## 4. BUOYANCY-DRIVEN FLOWS

Motivated by regions of disrupted ice on Europa's surface, known as chaos terrains, early work on Europa considered whether hydrothermal venting on the seafloor could lead to melt-through events at the satellite's surface (Thomson & Delaney 2001, Goodman et al. 2004, Goodman & Lenferink 2012). These plumes were envisioned to traverse the ocean in narrow columns confined by the Coriolis force, a consequence of the Taylor–Proudman theorem, where rapid rotation limits shearing in the direction parallel to the rotation axis. While melt-through events are not favored energetically (e.g., Lowell & DuBose 2005, Vance & Goodman 2009), the feasibility of columnar plumes extending across the ocean remains debated. Central to this debate are the degree to which

**Rayleigh number (*Ra*):** the ratio of buoyancy to diffusion

**Ekman number (*E*):** the ratio of viscous force to Coriolis force

**Prandtl number (*Pr*):** the ratio of momentum to thermal diffusivities

**Convective Rossby number ($Ro_c$):** the ratio of thermal wind velocity to free-fall velocity

**Natural Rossby number ($Ro^*$):** the ratio of rotational timescale to buoyancy timescale

rotation organizes the flow into vertical convection columns and how ocean salinity may limit their ascent, as discussed below.

The question of hydrothermal vents and their oceanic manifestation is not limited to Europa; it is also of fundamental importance for Enceladus, given the nature of ejected materials from its south pole (e.g., Hsu et al. 2015, Kang et al. 2022a, Schoenfeld et al. 2023). Liquid water fluxes from the high-pressure ice layers of Titan and Ganymede have also been hypothesized (Kalousová & Sotin 2020, Kalousová et al. 2023), making plume dynamics important across known ocean worlds. Local convective dynamics are not isolated, however, and can have global consequences through the development of zonal (east–west) flows, meridional overturning circulations, and modulation of heat and salt flux patterns at the ice–ocean interface.

## 4.1. The Role of Rotation

In the limit of rapid rotation, where the leading-order force balance is between the Coriolis and pressure gradient terms, quasi-geostrophic turbulence associated with vertically stiff convection will lead to an inverse energy cascade and alternating zonal jets with prograde flow at the equator and with widths outside the equatorial region set by the Rhines scale (e.g., Heimpel et al. 2005, Ashkenazy & Tziperman 2021, Bire et al. 2022, Hay et al. 2023). As the influence of rotation decreases, convective turbulence becomes increasingly three-dimensional, which changes the mechanism of zonal wind generation. This change is typically associated with a relative increase in the influence of the inertial force, which enhances mixing in both the temperature and angular momentum fields. The resulting angular momentum homogenization leads to retrograde jets at large cylindrical radii and prograde jets closer to the rotation axis (e.g., Aurnou et al. 2007, Gastine et al. 2013). As demonstrated systematically by Soderlund (2019), among others, intermediate regimes also exist with multiple jets and retrograde equatorial flow. When rotation is no longer first order such that convection is largely isotropic, zonal flow generation can become insignificant (Gastine et al. 2013). As highlighted in **Figure 3**, significant debate exists in the literature about which convective regime or regimes are most relevant to icy ocean worlds (Soderlund et al. 2014; Soderlund 2019; Amit et al. 2020; Ashkenazy & Tziperman 2021; Bire et al. 2022; Kvorka & Čadek 2022; D.G. Lemasquerier, C. Bierson & K.M. Soderlund, manuscript in review). This debate stems predominantly from the inability to resolve turbulence across the relevant length and temporal scales, uncertainty in which scaling laws are most appropriate, and the fact that bulk dynamic and heat transfer behavioral transitions do not necessarily coincide (e.g., Cheng et al. 2018, Aurnou et al. 2020, Bire et al. 2022, Hawkins et al. 2023).

An array of latitudinal heat transfer configurations are also found as a function of buoyancy forcing, rotation rate, and fluid properties, characterized by the dimensionless Rayleigh (*Ra*), Ekman (*E*), and Prandtl (*Pr*) numbers. Kvorka & Čadek (2022) identified three regimes of cooling behaviors in a large suite of numerical thermal convection models that span at least one order of magnitude for each *Ra*, *E*, and *Pr* as well as both no-slip and free-slip mechanical boundary conditions, encompassing the models of Soderlund (2019) and Amit et al. (2020). Polar cooling, where heat flux at the upper boundary peaks at high latitudes, is limited to a relatively narrow band of parameter space where the modified transitional number falls in the range $Ra^*_G = RaE^{12/7}Pr^{-1} \in \langle 1, 10 \rangle$, with equatorial cooling outside this range. It is worth noting that these transitions exhibit some sensitivity to mechanical boundary conditions and do not correspond with the commonly used convective Rossby number ($Ro_c$) (e.g., Aurnou et al. 2020), which is closely related to the natural Rossby number ($Ro^*$) (e.g., Bire et al. 2022). The thermal convection simulations by Bire et al. (2022) additionally indicate that the relative thickness of the ocean is also significant for the characteristics of heat transfer.

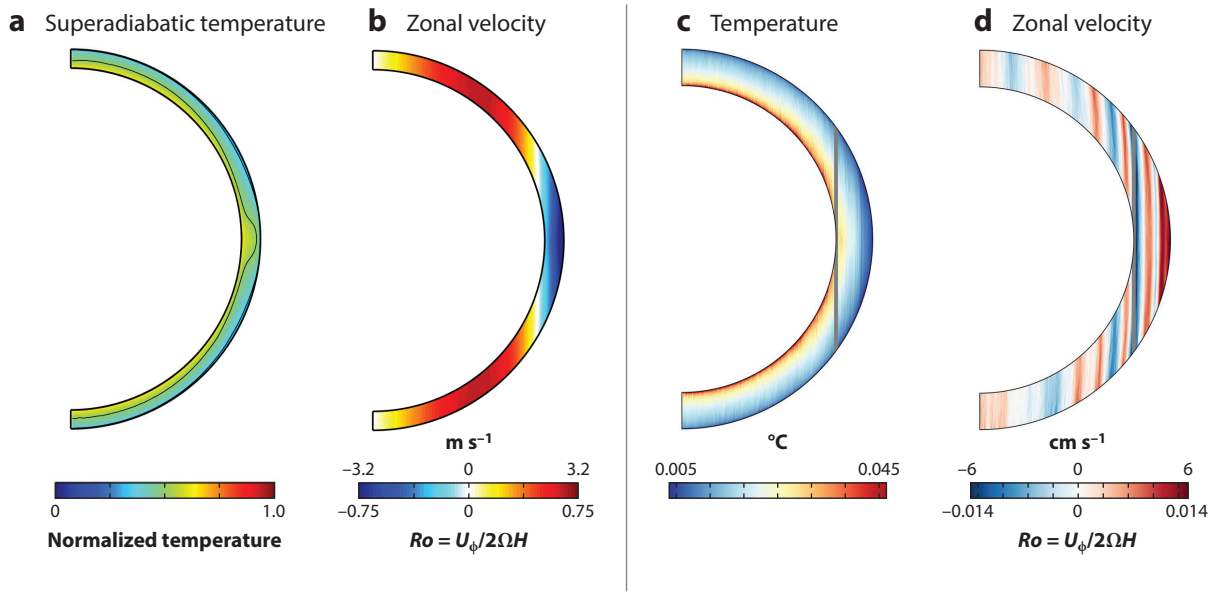


**Figure 3**

Simulated configurations of Europa's ocean from two proposed models. (*a*,*b*) Mean superadiabatic temperature normalized by the vertical contrast across the ocean (panel *a*) and mean zonal velocity as a function of radius and latitude (panel *b*) from a direct numerical simulation. (*c*,*d*) Mean temperature (panel *c*) and mean zonal velocity (panel *d*) from a large-eddy simulation. For both models, red (blue) denotes warm (cool) temperatures and prograde (retrograde) zonal flows. Velocities are given in dimensional units above the color bar and in dimensionless Rossby number (*Ro*) units below. The comparison between temperature plots should focus on their respective patterns rather than quantitative values, which should not be compared one-to-one between the models. Panels *a* and *b* adapted from Soderlund (2019) (CC BY 4.0); panels *c* and *d* adapted with permission from Bire et al. (2022) (CC BY-NC-ND 4.0).

Heat flux into the ocean may also not be spatially uniform (e.g., Choblet et al. 2017a,b; Běhounková et al. 2021). This has been investigated for global-scale variations associated with tidal heating (Lemasquerier et al. 2022; D.G. Lemasquerier, C. Bierson & K.M. Soderlund, manuscript in review) as well as smaller spatial scales associated with convection in the underlying region (rocky core or high-pressure ice layer) (Kang et al. 2022a, Terra-Nova et al. 2023). It appears that global-scale basal heat flux anomalies can be translated efficiently to the upper boundary, although the length scale where this translation becomes negligible remains unclear.

## 4.2. The Role of Ocean Salinity

The thermal properties of water affect buoyant flows by changing its density, but ocean salinity can have an even stronger control on ocean dynamics. The thermal expansivity of water is negative at low pressures and low salinity, such that the point of maximum density can occur at a temperature warmer than the freezing point. Although the density difference is small in these limited conditions, warming of the fluid counterintuitively increases its density, and cooling decreases its density, meaning cold water rises (Townsend 1964).

If the ocean salinity is low, at pressures relevant to part of Europa's hydrosphere and the entirety of Enceladus and other small moons, this anomalous density contrast driven by thermal expansion is more significant than for deeper oceans [Vance & Goodman 2009; Lawrence 2022; J.D. Lawrence, B.E. Schmidt, P.M. Washam, J.J. Buffo, C. Chivers & S.M. Miller, manuscript in review (hereafter cited as Lawrence et al., in review)]. From this, Melosh et al. (2004) suggested

that a buoyant "stratosphere" could develop in the ocean where upwelling motions are inhibited from the ice–ocean interface. Depending on the degree of underlying turbulence, this layer may be eroded away, which depends on the competition between the erosion rate (a mechanical forcing) and the cooling rate of the stable layer that restores its buoyancy. In addition, ice formation at the interface driven by this cold ventilation could create brine rejection that would further erode the layer or drive mixing that could disrupt the stratification.

While originally proposed for Europa, this phenomenon is especially pertinent to Enceladus (e.g., Soderlund 2019; Zeng & Jansen 2021; Kang et al. 2022b; Lawrence et al., in review). If a stable layer were to persist, it would suppress heat transfer to the ice shell and delay the transport of tracers that would need to be diffused rather than advected. The detection of nanosilicate particles in Enceladus's plume suggests that ice–ocean–rock exchange occurs, and furthermore, their size implies a short transport timescale on the order of months to years (Hsu et al. 2015), which is supported by convective particle entrainment calculations (Schoenfeld et al. 2023).

However, this density change due to thermal expansivity is also pressure dependent, such that the mass of the planet and radius of the ice shell affect the sign of $\alpha$. The role of pressure is important as it changes the point at which the ice shell and ocean can exchange mass through melting via freezing-point depression, or refreezing through supercooling. The adiabatic lapse rate determines the change in temperature that is incurred by a parcel of water moving from one depth to another, in the absence of heat or material exchange with the surrounding environment, and scales with gravity. For ocean worlds, this means that the freezing-point depression is more significant for larger planets and thicker ice—i.e., a parcel of water traversing a 1-m change in depth on Earth would experience the same change as it does over 8.5 m on Europa and ~85 m on Enceladus (Lawrence 2022; Lawrence et al., in review). All things being equal, this means that more significant topography or thickness variations can be maintained by the ice shells of smaller ocean worlds than on Europa, Ganymede, or Titan, which is consistent with the variability of Enceladus's ice shell (e.g., Čadek et al. 2019). It also means that the regime of ice–ocean interactions may change over time as the ice-shell thickness changes (Lawrence 2022; Lawrence et al., in review). Kang & Jansen (2022) arrived at similar conclusions using ocean circulation models. They found that large icy moons with strong gravity tend to have stronger ocean heat transport under the same ice-shell topography, leading to an equilibrium ice-shell geometry that is flatter on larger moons than it is on smaller ones.

On Earth, freezing-point suppression under ice shelves creates an exchange of material through both melting and ice production. Under roughly equilibrium conditions, such as those found beneath the Ross Ice Shelf, Antarctica, where the ocean temperatures are always near the freezing point and the regional circulation is heavily dependent on thermohaline processes, melting of deeper ice is balanced by freezing at shallower depths via marine ice accretion (direct freezing onto the ice-shelf base) or frazil- and platelet-ice production (free-floating ice crystals in the water column formed from relief of supercooling) (e.g., Lewis & Perkin 1986, Wolfenbarger et al. 2022). This process is known as the ice pump, and ice formation acts to erode topographic differences across the ice shelf, filling in crevasses (e.g., Lawrence 2022, Lawrence et al. 2023), affecting the base of thinner regions of the ice shelf hundreds of kilometers away (Koch et al. 2015), and influencing sea-ice formation and the sub-ice platelet-ice layer (Robinson et al. 2014). The ratio $\alpha\Delta T/\beta\Delta S$ describes whether an environment produces melting or refreezing (Lawrence 2022; Lawrence et al., in review), and ice pumps can form when $\alpha\Delta T/\beta\Delta S < 1$, as occurs under ice shelves (**Figure 4**). On the other hand, for low salinity but high pressures, a narrow regime in which $\alpha\Delta T/\beta\Delta S > 1$ exists where salinity does not control buoyancy. **Figure 4** shows that all but the very freshest oceans and deepest ice-shell depths for Ganymede and Titan would permit an ice pump to form.

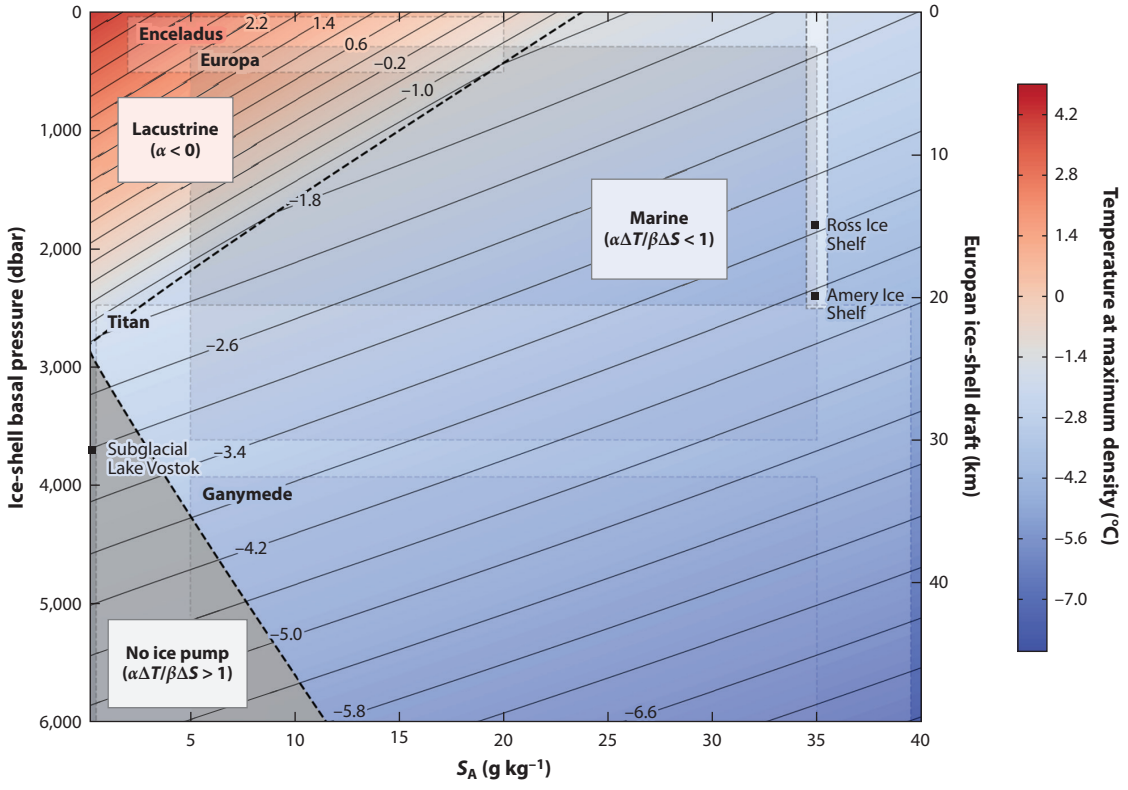


**Figure 4**

Three ice–ocean interaction regimes, determined by the temperature of maximum density and $\alpha\Delta T/\beta\Delta S$ upon meltwater mixing. In the lacustrine regime, $\alpha$ is negative and both $\Delta T$ and $\Delta S$ upon melting contribute to positive buoyancy, and ice pumping occurs. In the marine regime, $\alpha$ is positive, but $\beta$ dominates, and the freshening effect upon melting causes ice pumping. The white shaded rectangle indicates observed pressure and salinity ranges for sub-ice-shelf oceans in the marine regime (the Ross Ice Shelf and Amery Ice Shelf). At higher pressures and lower salinities, where $\alpha$ is positive, however, the ocean is too fresh for the dilution from melt input to overcome the temperature change, and no ice pumping occurs (e.g., subglacial Lake Vostok beneath the East Antarctic Ice Sheet). Ranges for ice–ocean interface pressures and ocean salinities are approximated with shaded regions for Enceladus, Europa, Ganymede, and Titan. Figure adapted with permission from Lawrence (2022).

Some recent progress has been made in capturing such ice–ocean interactions in planetary ocean models, but none of these models are complete. Ashkenazy & Tziperman (2021) used large-eddy simulations of Europa's ocean and included the effects of melting and freezing of the ice shell, finding that Taylor columns, alternating zonal jets with prograde flow at low latitudes, colder equatorial waters, and a nearly uniform ice-shell thickness are driven by an $\alpha\Delta T/\beta\Delta S$ ratio much less than unity. For Enceladus, in steady state, large variations in the ice shell would be required to drive melting or refreezing. While these variations must be maintained against viscous relaxation, ice flow is also likely slow due to low gravity and cold temperatures through much of the ice. Since both thermal and compositional buoyancy would aid in the production of a freshened upper layer, the resulting density structure in the shallow ocean leads to a meridional overturning circulation with a lens of relatively fresh water below the thinnest ice at the south pole (Lobo et al. 2021). The structure of this circulation depends on the magnitude and meridional extent of stable stratification in the ocean (e.g., Kang et al. 2022b).

While the above studies have considered both compositional and thermal buoyancy anomalies, they have not taken their different diffusion rates into account (i.e., double-diffusive convection). If the temperature gradient is unstable but the salinity gradient is stabilizing, a so-called diffusive regime develops that can form staircased layers. Conversely, if the temperature gradient is stable but the salinity gradient in destabilizing, finger plumes may develop. Wong et al. (2022) demonstrated that layering by double-diffusive convection is possible in Europa's ocean, although this layering may be transient depending on the amplitudes of the buoyancy anomalies. Vertical ocean transport efficiency would be reduced while such layers are present.

## 5. MECHANICALLY DRIVEN FLOWS

Tides raised by the gravitational pull of the planet and other moons in the system can significantly deform icy moons, producing tidal torques that change the spin of the moon. Precisely measuring the spin state and tidal deformations of a moon allows evaluation of its internal structure. While early studies assumed oceans to be an inviscid, static layer that transfers pressure between the crust and deep interior (e.g., Van Hoolst et al. 2008), tides and changes in the spin might generate intense flows that can significantly alter the tidal and rotational response of the moon and contribute to the heat budget.

Although tides and spin changes are intimately coupled, flows driven by tides and rotation have largely been studied separately. For the former, changes in the spin state from tidal torques are ignored; for the latter, the tidal bulge is assumed to be stationary and the geometry of the ocean is assumed to remain unchanged (rigid shell and mantle/core).

### 5.1. Tides

The orbit and spin of icy moons result in periodic changes of the tidal potential, driving ocean flows.

**5.1.1. The tidal potential.** The tidal potential can be expanded as a Fourier series and in terms of spherical harmonics, with each component characterized by its frequency $\omega$ and spherical harmonic degree $n$ (total wavenumber) and order $m$ (zonal wavenumber). The amplitude of tidal components quickly decreases with increasing degree; hence, it is common to consider only degree 2 terms. The leading term in the tidal potential is a degree 2, order 2 component and has an amplitude $\propto \Omega^2 R^2$, where $\Omega$ is the moon's rotation rate. For synchronous bodies, we expect a static tide that produces a permanent tidal bulge and does not directly drive ocean currents. The remaining terms are the result of the moon's nonzero eccentricity $e$ and obliquity $\theta_O$ (i.e., the inclination of the moon's rotational axis with respect to the orbital plane). The leading terms have a frequency $\Omega$ and amplitudes $\propto \Omega^2 R^2 e$ and $\propto \Omega^2 R^2 \sin\theta_O$, known as the eccentricity and obliquity tides, respectively. The eccentricity tide contains $m = 0$ and $m = 2$ components arising from the change in moon–planet distance and from the longitudinal variation of the subplanet point throughout one orbit, respectively. Obliquity tides only have an $m = 1$ component, which follows from the latitudinal libration of the subplanet point. Both eccentricity and obliquity tides can be split into westward- and eastward-propagating components. The next-in-order terms are often ignored given the small eccentricity and obliquity of icy moons (**Supplemental Tables 1 and 2**) (a complete expansion of the tidal potential for planet tides is given in Renaud et al. 2021). Other moons in the system also raise tides (Hay et al. 2020). As the moons' mass is much smaller than that of the planet, the amplitude of moon–moon tides is lower than that of planet tides. However, moon–moon tides have a richer frequency spectrum and introduce additional notes into the tidal response.

Supplemental Material >

**5.1.2. The Laplace tidal equations.** Most works on icy-moon ocean dynamics have relied on the LTEs (Equation 4), and the ocean's response can be understood in terms of eigenmodes. The excitation of the modes depends on the spatial structure and frequency of the tidal force and a series of nondimensional parameters (e.g., Rovira-Navarro et al. 2023). For a non-self-gravitating surface ocean overlying a rigid mantle/core, the tidal response is controlled by the Lamb parameter: $\epsilon = \Omega^2 R^2/gH$. For small $\epsilon$, two types of modes can be distinguished: class 1 and class 2 modes with eigenfrequencies given by, respectively, $\omega^2/\Omega^2 = n(n+1)/\epsilon$ and $\omega/\Omega = 2m/(n(n+1))$. Class 1 modes are surface gravity waves modified by rotation, with gravity acting as the restoring force; class 2 modes, also known as Rossby waves, arise due to the variations of the Coriolis force with latitude.

For icy moons, $\epsilon$ is much less than 1, which implies that resonant surface gravity waves are excited if $\omega^2/\Omega^2$ is much greater than 1. This is not the case for planet tides that have a characteristic frequency of $\Omega$, which implies that resonant gravity modes would be excited only if subsurface oceans were much thinner ($\lesssim$1 km). On the other hand, the frequency of some of the components of moon–moon tides is much higher. Because of this, moon–moon tides can resonantly excite the ocean, leading to energy dissipation that can exceed radiogenic heating and other tidal sources (Hay et al. 2020) and have distinct observational signatures (Hay et al. 2022). Away from resonances, the ocean response is well approximated by the equilibrium tide; the ocean adjusts almost immediately to changes in the geoid ($\eta_s = -\phi'/g$), and both characteristic flow velocities and tidal heating are small. Relaxing the massless and rigid-mantle/core assumptions (see **Table 1**) modifies the resonant condition and increases the amplitude of the equilibrium tide, which can now be written in terms of a degree-dependent admittance $Z_n$, $\eta_s = -Z_n\phi'_n/g$ (Matsuyama 2014, Matsuyama et al. 2018). An ice shell does not suppress surface gravity waves. The effect of the overlying ice shell depends on the moon's effective rigidity, $\gamma = 2\mu_{ice}(1+\nu_{ice})H_{ice}/g\rho_{ice}R^2$, with $\mu_{ice}$ the shear modulus and $\nu_{ice}$ the Poisson's ratio of ice (Beuthe et al. 2016, Matsuyama et al. 2018). For moons with a low effective rigidity, $\gamma \lesssim 1$ (soft-shell moons), the overlying ice shell has a small effect on the ocean's tidal response, while the opposite applies to moons with a high effective rigidity (hard-shell moons). In terms of gravity wave resonances, the effective rigidity increases the eigenfrequencies of surface gravity waves, reducing the strength of planet tides (**Figure 5**). The ice shell also decreases the admittance $Z_n$ so that $\gamma \to \infty$, $Z_n \to 0$.

The westward component of the obliquity tide can excite Rossby waves. For an ice-free, inviscid ocean, Rossby waves are divergence free ($\eta_s = 0$), and their amplitude is independent of ocean thickness and proportional to the moon's obliquity (Tyler 2008). Rossby waves can drive strong ocean currents provided the moon's obliquity is high (e.g., 0.1 m $s^{-1}$ for Europa provided its obliquity is 0.1°) and lead to energy dissipation higher than dissipation in the moon's solid layers (**Figure 5**). Except for Titan, the obliquity of icy moons has not been measured. Obliquity can be estimated assuming that the moon is in a Cassini state (Chen et al. 2014). From these estimations, it has been suggested that Rossby waves are relevant for Europa's (Tyler 2014) and Triton's (Nimmo & Spencer 2015) subsurface oceans and in the orbital evolution of Callisto (Downey et al. 2020). However, the above conclusions apply to oceans of constant thickness. Ocean thickness variations alter the eigenfrequency of Rossby waves and hinder their excitation by obliquity tides (Rovira-Navarro et al. 2023).

**5.1.3. Beyond the Laplace tidal equations.** LTE use is often justified by the small value of the ratio between ocean thickness and the characteristic length scale of the tidal force (the body's radius) and the fact that the ocean is experiencing vigorous convection that precludes the formation of a density gradient. However, the ratio between ocean thickness and radius is as high as $\sim 2{\cdot}10^{-1}$ for some icy moons, subsurface oceans could be partially stratified (see Section 4), and flow instabilities might be caused by tides.

**Lamb parameter ($\epsilon$):** the ratio between the squares of the speeds at which the tidal perturbation and surface gravity waves propagate

**Cassini state:** a rotational state in which the rotation and orbital periods are equal, the rotation axis has a constant inclination with respect to the ecliptic, and the three axes related to spin, orbit, and precession are coplanar

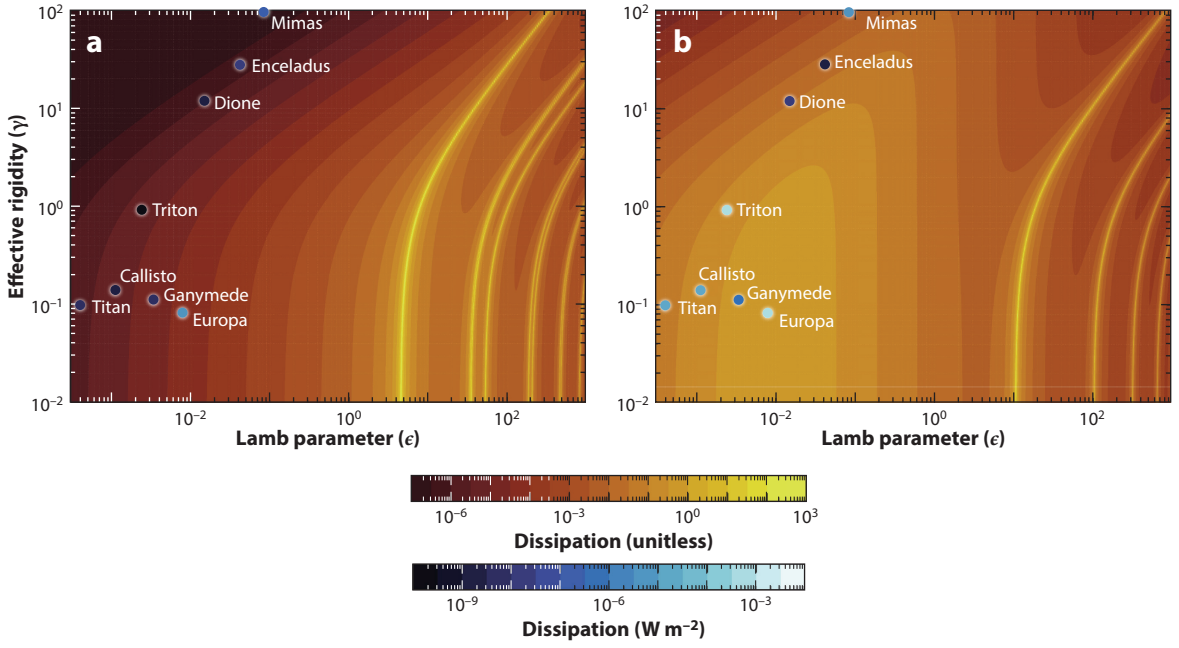


**Figure 5**

Nondimensional tidal heating due to the (*a*) eccentricity tide and (*b*) obliquity tide. Dimensional tidal heating for some icy moons is indicated. In all cases, self-gravity is ignored and a rigid core assumed. Tidal heating depends on the linear-drag coefficient; here, $\alpha_R/\Omega = 10^{-3}$ is employed. Regions of intense energy dissipation (*yellow areas*) are associated with strong ocean currents. Figure adapted from Rovira-Navarro et al. (2023) (CC BY 4.0).

Wave motions beyond the LTEs can be studied using a linearized version of Equation 4. The stratification of the ocean in density and angular momentum makes it possible for internal gravito-inertial waves to be excited. The properties of these waves are markedly different from those of surface gravity and Rossby waves (Maas 2005). If the ocean is unstratified in density, only internal inertial waves can be excited. Internal inertial waves propagate at a constant angle with respect to the rotational axis, $\arcsin(\omega/2\Omega)$, which for diurnal tides equals 30°. Upon reflection, this angle remains constant, but the wavelength might change. Depending on the ocean's geometry, this can lead to wave focusing; waves converge toward some particular trajectories, known as wave attractors (Rieutord et al. 2001). The shape of the attractor depends on the forcing frequency and the radius ratio between the ocean's bottom and top. For an inviscid ocean, a singularity arises along wave attractors in which velocity grows unbounded. An additional singularity also develops at the critical latitude (Stewartson & Rickard 1969). When the nonzero viscosity of the ocean is considered, these singularities give rise to internal shear layers where substantial energy can be dissipated (Rieutord et al. 2001). Rovira-Navarro et al. (2019) and Rekier et al. (2019) showed that the flow fields of Europa and Enceladus may be dominated by rays emanating from the critical latitude that might feed an attractor. The amount of energy dissipation within the shear layers varies by orders of magnitude depending on the ocean geometry but remains well below the amount of radiogenic and tidal heat generated in the solid layers.

**Critical latitude:** the ocean bottom latitude where the excited internal wave ray is tangent to the bottom ocean boundary

If the ocean is also stratified in density, the full complexity of gravito-inertial waves comes into focus. The modes excited by the tidal force depend on the stratification structure and the forcing and rotational frequencies. Two types of modes can be distinguished: short-wavelength modes, which feature prominent internal shear layers, and long-wavelength modes, which do

not feature internal shear layers (Dintras et al. 1999). The short-wavelength modes are similar to those discussed for internal inertial waves. However, while the wave attractors characteristic of internal inertial waves span the whole domain, for gravito-inertial modes, wave attractors are curbed and fill only parts of the fluid domain. Further insight can be obtained using the shallow-water approximation, which transforms Equation 3 into an LTE-type equation with an equivalent depth that depends on the ocean's stratification profile and is smaller than the total ocean depth (e.g., LeBlond & Mysak 1978). The eigenfrequencies of baroclinic modes are lower than those of surface gravity waves, allowing internal wave resonances to be excited by planet tides (Tyler 2011a). Using a simplified two-layer model, Rovira-Navarro et al. (2023) showed that internal gravity waves are more relevant for moons with high effective rigidity, such as Enceladus. Here, internal wave resonances can drive strong ocean currents ($\sim$1 m $s^{-1}$), and tidal heating can be as high as the moon's observed thermal output. Such strong currents challenge the linearization assumption. The velocity shear associated with the baroclinic mode further makes the system prone to the Kelvin–Helmholtz instability, which can lead to ocean mixing and hence result in complex feedbacks between buoyancy-driven and mechanically driven flows.

Note that in the discussion so far, internal waves are excited at the global scale by tidal forcing. A local excitation is also possible and could be due to, for example, the barotropic tide flowing across boundary topography. Such a mechanism is key to closing Earth's oceanic energy budget; it accounts for $\sim$30% of the total energy dissipated by ocean tides (e.g., Garrett & Kunze 2007, Xie et al. 2023). No study relevant for subsurface oceans, involving different shell thicknesses and topographies along both top and bottom boundaries as well as various relative amplitudes of stratification and rotation, has been performed so far. Focusing on the simple spin-up of a constant-density fluid, the seminal experiment of Burmann & Noir (2018), however, highlighted the primordial role of inertial waves radiated from boundary roughness.

Reintroducing nonlinearities in the momentum equation leads to even more complicated and poorly explored dynamics. Nonlinear self-interaction of a tidally excited internal wave can drive zonal flows (Tilgner 2007, Morize et al. 2010), whose associated shear might even become large enough to generate local turbulence (Favier et al. 2014, Sauret et al. 2014). Wave focalization around attractors or because of their interactions with an ambient mean flow might also lead to a strong increase in their amplitude and to breaking (e.g., Staquet & Sommeria 2002 for internal gravity waves). Finally, the tidal flow can trigger a so-called parametric instability involving two gravito-inertial waves, which are complementary in terms of wavenumbers and frequencies (e.g., Le Bars et al. 2015). Even if the tidal excitation is of small amplitude, the resonant feature of this tidal instability might result in intense, three-dimensional flows whose saturation is still debated (Le Reun et al. 2017, 2018). For now, these various nonlinear tidal processes have been studied either in local theoretical models that ignore boundaries (e.g., Barker & Lithwick 2013) or in global experimental and numerical models in idealized geometries, including a few in deep spherical shells (e.g., Aldridge et al. 1997, Lacaze et al. 2005). Their assessment in the thin spherical shell geometry relevant for icy satellite oceans remains a challenging prospect, mainly because the overwhelming viscous dissipation in accessible laboratory and computer regimes renders the fully turbulent state inaccessible. Also, while these tidal flows still operate in the presence of convection (Cébron et al. 2010, de Vries et al. 2023), the interactions of these possibly simultaneous processes deserve additional studies.

### 5.2. Spin-Driven Flows

In addition to tidal distortions of the ocean boundaries, gravitational interactions of the moon with its planet and neighbors also induce periodic modification of its spin rate and spin direction, respectively corresponding to libration and precession mechanical forcing.

**Ekman layer:** the boundary layer in which the momentum equation experiences balance between the viscous force and Coriolis acceleration

**Stewartson layer:** a detached shear layer in a rotating container, whose general structure and thickness depend on the Ekman number

**Tangent cylinder:** an imaginary right cylinder tangent to the ocean's bottom boundary at the equator

**5.2.1. Libration.** The tidal bulge supports a periodic torque along the elliptical orbit, tending to realign it with the central planet. This produces a small oscillation of the moon's spin called physical longitudinal libration. For synchronously rotating moons, the libration frequency equals the orbital and mean rotational frequencies, but a rich libration spectrum settles in from gravitational couplings with other neighboring bodies (e.g., Richard et al. 2014). In structural libration models, ocean flow is neglected: The fluid follows a simple solid-body rotation independent of the libration of its boundaries. This is indeed the largely dominant flow. Yet libration might generate intense flows and dissipation in the liquid ocean, hence significantly contributing to its heat budget. As described below and in more detail by Le Bars et al. (2015), a large variety of flows are possible depending on the moon spin, orbit, mass, and so on. These intense flows might be located in the ocean boundary layers (i.e., near the ice–ocean interface or the ocean–mantle/core interface) or in the ocean bulk. Also, these flows might reach a turbulent quasi-steady state or involve successive cycles of growth and collapse.

Librating the solid boundary of a rotating fluid induces successive spin-up and spin-down phases through time. Let us first consider an axisymmetric geometry: Coupling between solid and liquid is viscous only, and for a rapidly rotating fluid, it is contained in the thin Ekman boundary layer. Hence, the spin-up and spin-down of the solid boundary are felt only within this Ekman layer, where it propagates by viscosity from the no-slip boundary, while the bulk fluid outside the Ekman layer keeps rotating at its initial spin. The laminar torque associated with this differential rotation is the dominant cause of dissipation at the linear order in Enceladus (Rekier et al. 2019) even if it remains largely insufficient to explain the endogenic heat flow measured by *Cassini*.

These oscillating boundary flows, however, are prone to centrifugal instability, a classical instability occurring in a homogeneous fluid owing to the dynamical effects of rotation and of streamline curvature (e.g., Drazin & Reid 2004); boundary flows can then become turbulent. This mechanism has been studied by Noir et al. (2009), who showed the emergence of longitudinal rolls and then boundary turbulence above some given threshold in terms of libration amplitude, defined as the product of the libration frequency and the maximum angular displacement. Enceladus and numerous moons actually fall in the turbulent regime, leading to strongly increased heating; while the exact quantification of this turbulent dissipation is still unknown, Wilson & Kerswell (2018) provided a rigorous upper bound that would fulfill *Cassini* measurements when the effects of tidal distortion and boundary roughness are included.

In addition to boundary-layer flows, libration of an axisymmetric container can also resonantly excite internal waves that propagate in the system bulk. This mechanism has been observed in rotating experiments both in a sphere (Aldridge & Toomre 1969) and in spherical shells (Koch et al. 2013, Hoff et al. 2016, Lemasquerier et al. 2017). The works on spherical shells reported more intense inertial mode resonances in the shells thanks to energy focusing toward wave attractors, as already described for tidal forcing. Yet Zhang et al. (2013) have challenged the efficiency of the libration resonant excitation in the limit of low viscosity and small libration amplitude, so the applicability of direct wave forcing in axisymmetric oceans remains open. For instance, Rekier et al. (2019) did not notice any significant resonance in their linear, laminar, axisymmetric libration models. Note, however, that turbulent Ekman layers can efficiently excite waves, even for a driving libration frequency beyond the frequency range of internal wave existence (Sauret et al. 2013).

Libration studies in spherical shells (Koch et al. 2013, Hoff et al. 2016, Lemasquerier et al. 2017) also systematically reported the emergence of a prograde, geostrophic zonal jet within the Stewartson layer (Stewartson 1966) along the tangent cylinder. Geostrophic jet formation is a generic process due to the nonlinear self-interaction of any oscillating flow. In addition to internal boundary-layer flows that produce the Stewartson jet, nonlinear self-interaction of oscillatory flows and geostrophic jet formation also take place in the outer boundary layer of librating systems

(Busse 2010, Sauret et al. 2010) and in the bulk flow associated with internal waves (Calkins et al. 2010). The torques and dissipation associated with those zonal flows and their consequences for the celestial motions of planets and moons remain to be investigated. Even more interesting for dissipation, these jets become unstable at sufficiently large forcing amplitudes, generating bulk filling turbulence (Hoff et al. 2016).

As for tidal flows, accounting for non-axisymmetry of the ocean leads to even more intense and complex flows. All processes described above persist; resonant wave and zonal flow excitations are amplified by the topographic forcing (e.g., Noir et al. 2012, Rekier et al. 2019). In ellipsoidal shells, libration can also excite a so-called parametric instability, similar to the one described in the previous section for tidal forcing. The basic mechanism for instability is a resonance between two internal waves of the system and the libration base flow in the bulk induced by topographic coupling (for details, see Le Bars et al. 2015). This instability exponentially grows and saturates in a complex turbulent state made of a superposition of columnar structures, wavy patterns, and overturning flows (e.g., **Figure 6**). Quantification of turbulent saturation is a forthcoming challenge to fully appreciate the role of libration in subsurface oceans. In fact, this question echoes the broader, long-standing issue of rotating turbulence (Godeferd & Moisy 2015), where two different models, the strong and weak turbulence models, interact and compete (the same is true for stratified flows but is not detailed here; see Brouzet et al. 2016). In the strong turbulence model (i.e., for strong forcing), the flow is quasi-geostrophic and concentrates in large columnar structures aligned with the rotation axis following an inverse energy cascade (see also Section 4.1). In

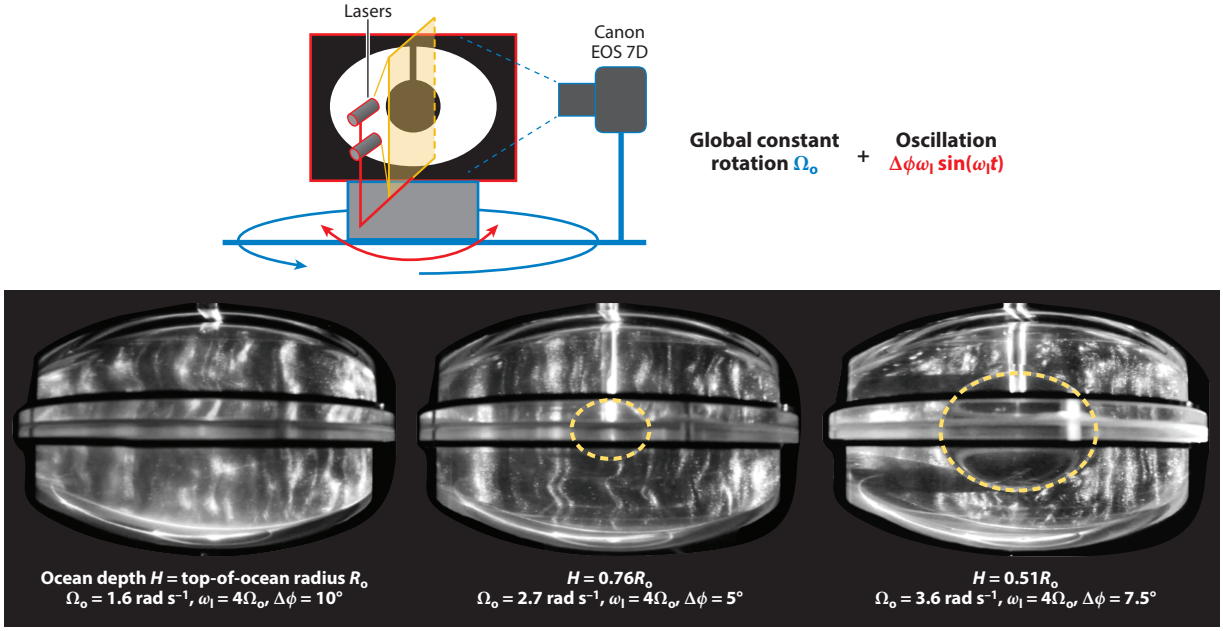


**Figure 6**

Experimental setup and visualizations of turbulent flow in a meridional plane for a full ellipsoid and two different ellipsoidal shells (the rigid inner cores are highlighted by *yellow dotted curves*). Strong vertical shear zones and superposed wavy patterns are visualized in a laser sheet by light reflection from small elongated flakes. These images were obtained for a libration frequency equal to four times the spin rate but different libration angles and rotation rates depending on the limits of the experimental setup. More cases and details are given by Lemasquerier et al. (2017) (in particular, see their figure A1). The purpose here is to illustrate that the turbulent state persists no matter what the ocean depth is. Figure adapted from Lemasquerier et al. (2017).

the weak turbulence model (i.e., for small forcing), energy transfers through successive triadic internal wave resonances that extend the parametric resonance instability described above, leading to a fully three-dimensional state. The predominance of geostrophic versus wave turbulence in subsurface oceans remains an open question, while both lead to very different estimates in terms of typical flow scales, torques, and dissipation (Le Reun et al. 2019).

Finally, most studies of libration-driven flows have considered an isodensity fluid; studies coupling libration and buoyancy effects are required to better assess their role in subsurface oceans. A priori, all previous results should apply to an adiabatic ocean efficiently mixed by a strong, small-scale convection, and they should also apply to a stably stratified ocean, replacing inertial waves with gravito-inertial ones. The other main remaining challenge is to develop fully coupled models involving both the nonlinear ocean dynamics and the evolution of the overlying ice crust, including its realistic tidal deformation and its local growth or melting following the spatiotemporal heat flux variations associated with oceanic turbulence.

**5.2.2. Precession.** Precession corresponds to the mechanical forcing associated with rotation of the spin axis of a planet or moon along the normal to the ecliptic. The amplitude of this forcing is equal to the product of the precession rate and the sine of the obliquity. Precession is assumed to be subdominant compared with tides and libration for driving present subsurface ocean flow. But this might have been different in the past, and precession can combine with libration and tidal instabilities to induce even stronger flows.

The fluid dynamics of precession has been historically studied because of its possible relevance for planetary core flows and dynamos (e.g., Malkus 1968). It is largely similar to the dynamics described above for other mechanical forcings, with some additional complexities and specificities [see the review by Le Bars et al. (2015)]. Precession first drives a Poincaré base flow, which consists of a solid-body rotation at a constant rate lagging behind the solid-boundaries motion. This Poincaré base flow can resonate with the internal eigenmodes of the fluid, in particular with the simplest one, called the spin-over mode or free core nutation by astronomers; this resonance then leads to strong differential rotation with the boundaries (Malkus 1968, Nobili et al. 2021). Second, precession excites internal waves that organize in oblique shear layers, whose nonlinear interactions, as well as nonlinear interactions in the boundary layers, drive intense axisymmetric geostrophic jets. Also, the shear between the fluid and the boundaries due to the Poincaré flow can drive turbulence in the Ekman layers, leading to significantly increased dissipation (Cébron et al. 2019). Finally, precession can excite a parametric instability, whose exact forcing mechanism is still controversial (Nobili et al. 2021). In spherical geometries, the forcing comes from the excited oblique shear layers (Lin et al. 2015). But when the polar flattening and the equatorial bulge of real planets and moons are accounted for, this conical shear instability competes with two other mechanisms described by Kerswell (1993), corresponding to the periodic shear and to the elliptical distortion of the rotating streamlines of the Poincaré flow in nonspherical domains. Note that the different mechanisms are not exclusive but may be present at the same time and interact with each other. As described for the libration case, the turbulent state of precession flows is still unknown.

## 6. ELECTROMAGNETICALLY DRIVEN FLOWS

A novel mechanism for driving ocean circulation based on coupling with Jupiter's magnetosphere has been hypothesized for Europa (Gissinger & Petitdemange 2019). Here, the tilt of the planet's dipolar magnetic field component causes the satellite to experience a periodic magnetic oscillation that drives fluid motions through a Lorentz force. These flows would be concentrated in a

retrograde equatorial jet and associated low-latitude meridional overturning. Ohmic dissipation within the ocean is also expected, although it is likely small compared with radiogenic and tidal heating. The resulting electromagnetic torque applied to the ocean depends on the phase lag between the planet's field and the satellite's induced magnetic field, and the resulting flow speeds are argued to depend on the planet's magnetic field strength at the satellite, so this effect decreases with increasing distance from the planet. Electromagnetic pumping may therefore be significant at Europa, small at Ganymede, and negligible at Callisto. In the Saturnian system, this effect is likely small due to the planet's nearly axisymmetric magnetic field. The large tilts of Uranus's and Neptune's dipolar magnetic field components would lead to a significant magnetic oscillation, but this oscillation would be offset by the weaker total field strength; the role of electromagnetic pumping is thus unclear for the Uranian and Neptunian systems and warrants further investigation.

## 7. PERSPECTIVES FROM EARTH

Observations from beneath terrestrial ice shelves suggest further lessons for planetary oceanography. In systems that are out of equilibrium—that is, where some process perturbs the temperatures in the upper ocean from the near steady state they generally experience—progressively fresher boundary layers may be built up over time due to ice melt without reaching the freezing point. This occurs because of the difference between the diffusion rates of heat and salt. However, advection of heat laterally also becomes important in such regimes and can drive widening of ice-shell topography, as opposed to deepening or erasing it. This has been observed in rapidly melting regions of Antarctic ice shelves (e.g., Dutrieux et al. 2014, Schmidt et al. 2023) and Petermann Glacier, Greenland (e.g., Washam et al. 2018).

Melting along ice surfaces is not uniform, but instead depends on stratification and turbulent heat flow. In fully turbulent conditions, the surface of melting ice shelves develops a characteristic golf-ball-like texture of scallops and other quasi-circular or elongated melt structures (e.g., Lawrence et al. 2023). These melted features create drag within the boundary layer. Such ice–ocean coupling can either inhibit or enhance boundary-layer-driven processes, depending on conditions.

Dynamics of plumes along ice–ocean interfaces are increasingly important for understanding Earth's cryosphere (e.g., Straneo & Cedenese 2015, Hewitt 2020) but thus far have not been studied in depth on planetary bodies. Consider a buoyant plume (say, a mixture of ocean water and meltwater sourced from deep draft ice) rising along a sloped ice–ocean interface. As the parcel moves up, increased buoyancy increases its rate of ascent; at the same time, this increased flow speed drives turbulence in the surrounding ocean, which drives mixing of the ocean water into the parcel. This feedback is key: Under the right conditions, the rising plume never actually reaches the ice–ocean interface and instead breaks away from the ice lower in the water column, driving further mixing and disrupting stratification. Other feedbacks among heat transport, ice slope and shape, current speed, and stratification can strongly influence how the ice and ocean exchange material and heat, affecting ocean dynamics as well as the ice (e.g., Lawrence et al. 2023, Schmidt et al. 2023). Depending on conditions, ice topography such as keels and crevasses can be erased (through freezing or melting) or enhanced (by melting).

These dynamics suggest complex and important feedbacks among temperature, composition, pressure, ice-shell thickness, and topography (on many scales) as well as circulation and mechanical forcing between the ice and the ocean, such that many of the simplifying assumptions made in studying planetary oceanographic regimes are unable to realistically constrain these interactions. In particular, the mass flux between the ice and the ocean, which is thought to be important in determining not only the interior structure of ocean worlds but also their habitability, may be

driven by these interactions. Moreover, stratification and topography strongly affect each other, as well as ocean circulation both locally and on broad scales, such that self-consistently capturing these phenomena will be an important future advance for both polar and planetary oceanography.

We further argue that the central iron-alloy core of Earth (and other planets) also provides a useful analog for planetary oceanography, as both Earth's core and planetary oceans are global reservoirs of a rotating, low-viscosity liquid (for a review of potential processes driving the geodynamo, see Landeau et al. 2022). Moreover, core convection is driven by both thermal and compositional buoyancy anomalies, which can operate in tandem or in opposing directions. Mechanically driven flows are also at play, especially for the early geodynamo. The modification of flows by magnetic fields is additionally a principal element. Indeed, many of the models and laboratory experiments presented above leveraged codes, experiments, and ideas developed by the deep-Earth community. The momentum for planetary oceanography will continue to accelerate in the decades ahead through such multidisciplinary collaborations.

## SUMMARY POINTS

1. Oceans beyond Earth are known to exist in at least four ice-covered moons in the outer solar system (Europa, Ganymede, Enceladus, and Titan), with observational hints for several others and theoretical possibilities for more still.
2. These oceans are rich dynamical systems with flows excited and modulated by buoyancy, tides, libration, precession, and electromagnetic pumping. Each driving mechanism is inherently complex and has its own permutations, so few studies have yet crossed these artificial boundaries.
3. Ice–ocean interactions, pertaining to the exchange of material, heat, and momentum, are a critical and as yet understudied part of the ocean-world system that requires tracking the full array of oceanographic processes.

## FUTURE ISSUES

1. Future missions to the outer solar system are in development to explore the habitability of Europa (*Europa Clipper*), Ganymede and the Jovian system more broadly [*Jupiter Icy Moons Explorer* (*Juice*)], and Titan (*Dragonfly*). Flagship-class missions to the Uranian system and Enceladus were also identified as high priorities in *Origins, Worlds, and Life: A Decadal Strategy for Planetary Science and Astrobiology 2023–2032* (Natl. Acad. Sci. 2022).
2. As these missions are being designed and launched, it is essential to develop testable hypotheses for ocean dynamics (e.g., ice-shell thickness variations, motional magnetic field induction, and nonsynchronous rotation).
3. For buoyancy-driven flows, future work should unite direct numerical simulations, large-eddy simulations, and laboratory experiments with theory to understand how convective processes operate at extreme (i.e., more realistic) input parameters.
4. For tidally driven flows, future work should explore the role of ice-shell and basal topography, push the parameter regime of numerical and laboratory experiments toward more realistic regions, and explore feedbacks between ocean tidal dissipation and the interior and orbital evolution of icy worlds.

5. For spin-driven flows, future work should study turbulence in the relevant parameter regime, the effect of boundary roughness, and combinations of forcings (e.g., tides in rotating and stratified flows, tides and libration, and libration and convection).
6. Work aimed at understanding the interactions and feedbacks among buoyancy-driven, mechanically driven, and electromagnetically driven flows is necessary to understand subsurface ocean dynamics (e.g., the role of ocean mixing in the ocean's overturning circulation) and to interpret data returned by future missions, which will reflect all driving mechanisms in aggregate.
7. Accurately coupled ice–ocean studies, which have critical implications for mass exchange between the ocean and ice, are a frontier for both Earth and planetary oceanographers. Better parameterizations for boundary flows, turbulent mixing, and heat and salt fluxes between these reservoirs are sorely needed, and realistic treatment of melting and freezing along dynamic ice-shell topography is crucial.
8. Without direct access to subsurface oceans, further exploration of Earth-analog environments and laboratory experiments at subsurface ocean conditions are key to provide required context for the physical oceanography of ice-covered moons.

## DISCLOSURE STATEMENT

The authors are not aware of any affiliations, memberships, funding, or financial holdings that might be perceived as affecting the objectivity of this review.

## ACKNOWLEDGMENTS

K.M.S. and B.E.S. were funded by the NASA Astrobiology program grant Oceans Across Space and Time (grant number 80NSSC18K1301). M.R.-N. was supported by NASA grant number 80NSSC20K0570 issued through the Solar System Workings program. M.L.B. acknowledges financial support from the French Agence Nationale de Recherche project ANR COLOSSe (grant number ANR-2020-CE49-0010).

## LITERATURE CITED

Aldridge KD, Seyed-Mahmoud B, Henderson G, van Wijngaarden W. 1997. Elliptical instability of the Earth's fluid core. *Phys. Earth Planet. Inter.* 103(3–4):365–74

Aldridge KD, Toomre A. 1969. Axisymmetric inertial oscillations of a fluid in a rotating spherical container. *J. Fluid Mech.* 37(2):307–23

Amit H, Choblet G, Tobie G, Terra-Nova F, Čadek O, Bouffard M. 2020. Cooling patterns in rotating thin spherical shells—application to Titan's subsurface ocean. *Icarus* 338:113509

Ashkenazy Y, Tziperman E. 2021. Dynamic Europa ocean shows transient Taylor columns and convection driven by ice melting and salinity. *Nat. Commun.* 12(1):6376

Aurnou JM, Heimpel MH, Wicht J. 2007. The effects of vigorous mixing in a convective model of zonal flow on the ice giants. *Icarus* 190:110–26

Aurnou JM, Horn S, Julien K. 2020. Connections between nonrotating, slowly rotating, and rapidly rotating turbulent convection transport scalings. *Phys. Rev. Res.* 2(4):043115

Barker AJ, Lithwick Y. 2013. Non-linear evolution of the tidal elliptical instability in gaseous planets and stars. *Mon. Not. R. Astron. Soc.* 435(4):3614–26

Bauer JM, Roush TL, Geballe TR, Meech KJ, Owen TC, et al. 2002. The near infrared spectrum of Miranda: evidence of crystalline water ice. *Icarus* 158(1):178–90

Beddingfield C, Burr D, Emery J. 2015. Fault geometries on Uranus' satellite Miranda: implications for internal structure and heat flow. *Icarus* 247:35–52

Běhounková M, Tobie G, Choblet G, Kervazo M, Melwani Daswani M, et al. 2021. Tidally induced magmatic pulses on the oceanic floor of Jupiter's moon Europa. *Geophys. Res. Lett.* 48(3):e2020GL090077

Beuthe M, Rivoldini A, Trinh A. 2016. Enceladus's and Dione's floating ice shells supported by minimum stress isostasy. *Geophys. Res. Lett.* 43(19):10088–96

Bierson CJ, Nimmo F. 2022. A note on the possibility of subsurface oceans on the Uranian satellites. *Icarus* 373:114776

Bire S, Kang W, Ramadhan A, Campin JM, Marshall J. 2022. Exploring ocean circulation on icy moons heated from below. *J. Geophys. Res. Planets* 127(3):e2021JE007025

Bland MT, Showman AP, Tobie G. 2009. The orbital–thermal evolution and global expansion of Ganymede. *Icarus* 200(1):207–21

Brouzet C, Ermanyuk EV, Joubaud S, Sibgatullin I, Dauxois T. 2016. Energy cascade in internal-wave attractors. *Europhys. Lett.* 113(4):44001

Burmann F, Noir J. 2018. Effects of bottom topography on the spin-up in a cylinder. *Phys. Fluids* 30(10):106601

Busse F. 2010. Mean zonal flows generated by librations of a rotating spherical cavity. *J. Fluid Mech.* 650:505–12

Čadek O, Souček O, Běhounková M, Choblet G, Tobie G, Hron J. 2019. Long-term stability of Enceladus' uneven ice shell. *Icarus* 319:476–84

Calkins MA, Noir J, Eldredge JD, Aurnou JM. 2010. Axisymmetric simulations of libration-driven fluid dynamics in a spherical shell geometry. *Phys. Fluids* 22(8):086602

Cartwright RJ, Beddingfield CB, Nordheim TA, Roser J, Grundy WM, et al. 2020. Evidence for ammonia-bearing species on the Uranian satellite Ariel supports recent geologic activity. *Astrophys. J. Lett.* 898(1):L22

Castillo-Rogez JC, Hemingway D, Rhoden A, Tobie G, McKinnon WB. 2018. Origin and evolution of Saturn's mid-sized moons. In *Enceladus and the Icy Moons of Saturn*, ed. PM Schenk, RN Clark, CJA Howett, AJ Verbiscer, JH Waite, pp. 285–305. Tucson: Univ. Ariz. Press

Castillo-Rogez JC, Weiss B, Beddingfield C, Biersteker J, Cartwright R, et al. 2023. Compositions and interior structures of the large moons of Uranus and implications for future spacecraft observations. *J. Geophys. Res. Planets* 128(1):e2022JE007432

Cébron D, Laguerre R, Noir J, Schaeffer N. 2019. Precessing spherical shells: flows, dissipation, dynamo and the lunar core. *Geophys. J. Int.* 219(Suppl. 1):S34–57

Cébron D, Maubert P, Le Bars M. 2010. Tidal instability in a rotating and differentially heated ellipsoidal shell. *Geophys. J. Int.* 182(3):1311–18

Chen E, Nimmo F, Glatzmaier G. 2014. Tidal heating in icy satellite oceans. *Icarus* 229:11–30

Cheng JS, Aurnou JM, Julien K, Kunnen RPJ. 2018. A heuristic framework for next-generation models of geostrophic convective turbulence. *Geophys. Astrophys. Fluid Dyn.* 112(4):277–300

Choblet G, Tobie G, Sotin C, Běhounková M, Čadek O, et al. 2017a. Powering prolonged hydrothermal activity inside Enceladus. *Nat. Astron.* 1(12):841–47

Choblet G, Tobie G, Sotin C, Kalousová K, Grasset O. 2017b. Heat transport in the high-pressure ice mantle of large icy moons. *Icarus* 285:252–62

Ćuk M, Dones L, Nesvorný D. 2016. Dynamical evidence for a late formation of Saturn's moons. *Astrophys. J.* 820(2):97

Ćuk M, Moutamid ME, Tiscareno MS. 2020. Dynamical history of the Uranian system. *Planet. Sci. J.* 1(1):22

de Vries NB, Barker AJ, Hollerbach R. 2023. The interactions of the elliptical instability and convection. *Phys. Fluids* 35(2):024116

Dintras B, Rieutord M, Valdettaro L. 1999. Gravito-inertial waves in a rotating stratified sphere or spherical shell. *J. Fluid Mech.* 398:271–97

Downey BG, Nimmo F, Matsuyama I. 2020. Inclination damping on Callisto. *Mon. Not. R. Astron. Soc.* 499(1):40–51

Drazin PG, Reid WH. 2004. *Hydrodynamic Stability*. Cambridge, UK: Cambridge Univ. Press

Dutrieux P, Stewart C, Jenkins A, Nicholls KW, Corr HFJ, et al. 2014. Basal terraces on melting ice shelves. *Geophys. Res. Lett.* 41(15):5506–13
Favier B, Barker A, Baruteau C, Ogilvie G. 2014. Non-linear evolution of tidally forced inertial waves in rotating fluid bodies. *Mon. Not. R. Astron. Soc.* 439(1):845–60
Garrett C, Kunze E. 2007. Internal tide generation in the deep ocean. *Annu. Rev. Fluid Mech.* 39:57–87
Gastine T, Wicht J, Aurnou JM. 2013. Zonal flow regimes in rotating anelastic spherical shells: an application to giant planets. *Icarus* 225:156–72
Gerkema T. 2019. *An Introduction to Tides*. Cambridge, UK: Cambridge Univ. Press
Gerkema T, Zimmerman JTF. 2008. *An introduction to internal waves*. Lect. Notes, R. Neth. Inst. Sea Res., Texel, Neth.
Gerkema T, Zimmerman JTF, Maas LRM, van Haren H. 2008. Geophysical and astrophysical fluid dynamics beyond the traditional approximation. *Rev. Geophys.* 46(2):RG2004
Gissinger C, Petitdemange L. 2019. A magnetically driven equatorial jet in Europa's ocean. *Nat. Astron.* 3:401–7
Godeferd FS, Moisy F. 2015. Structure and dynamics of rotating turbulence: a review of recent experimental and numerical results. *Appl. Mech. Rev.* 67(3):030802
Goodman JC, Collins GC, Marshall J, Pierrehumbert RT. 2004. Hydrothermal plume dynamics on Europa: implications for chaos formation. *J. Geophys. Res.* 109:E03008
Goodman JC, Lenferink E. 2012. Numerical simulations of marine hydrothermal plumes for Europa and other icy worlds. *Icarus* 221:970–83
Green JAM, Nycander J. 2013. A comparison of tidal conversion parameterizations for tidal models. *J. Phys. Oceanogr.* 43(1):104–19
Hartkorn O, Saur J. 2017. Induction signals from Callisto's ionosphere and their implications on a possible subsurface ocean. *J. Geophys. Res. Space Phys.* 122(11):11677–97
Hawkins EK, Cheng JS, Abbate JA, Pilegard T, Stellmach S, et al. 2023. Laboratory models of planetary core-style convective turbulence. *Fluids* 8(4):106
Hay HCFC, Fenty I, Pappalardo RT, Nakayama Y. 2023. Turbulent drag at the ice-ocean interface of Europa in simulations of rotating convection: implications for nonsynchronous rotation of the ice shell. *J. Geophys. Res. Planets* 128(3):e2022JE007648
Hay HCFC, Matsuyama I. 2017. Numerically modelling tidal dissipation with bottom drag in the oceans of Titan and Enceladus. *Icarus* 281:342–56
Hay HCFC, Matsuyama I, Pappalardo RT. 2022. The high-frequency tidal response of ocean worlds: application to Europa and Ganymede. *J. Geophys. Res. Planets* 127(5):e2021JE007064
Hay HCFC, Trinh A, Matsuyama I. 2020. Powering the Galilean satellites with moon-moon tides. *Geophys. Res. Lett.* 47(15):e2020GL088317
Heimpel MH, Aurnou JM, Wicht J. 2005. Simulation of equatorial and high-latitude jets on Jupiter in a deep convection model. *Nature* 483:193–96
Hemingway DJ, Iess L, Tajeddine R, Tobie G. 2018. The interior of Enceladus. In *Enceladus and the Icy Moons of Saturn*, ed. PM Schenk, RN Clark, CJA Howett, AJ Verbiscer, JH Waite, pp. 57–78. Tucson: Univ. Ariz. Press
Hewitt IJ. 2020. Subglacial plumes. *Annu. Rev. Fluid Mech.* 52:145–69
Hoff M, Harlander U, Egbers C. 2016. Experimental survey of linear and nonlinear inertial waves and wave instabilities in a spherical shell. *J. Fluid Mech.* 789:589–616
Hofgartner JD, Birch SP, Castillo J, Grundy WM, Hansen CJ, et al. 2022. Hypotheses for Triton's plumes: new analyses and future remote sensing tests. *Icarus* 375:114835
Hsu HW, Postberg F, Sekine Y, Shibuya T, Kempf S, et al. 2015. Ongoing hydrothermal activities within Enceladus. *Nature* 519:207–10
Hussmann H, Spohn T. 2004. Thermal-orbital evolution of Io and Europa. *Icarus* 171(2):391–410
Ingersoll AP. 2005. Boussinesq and anelastic approximations revisited: potential energy release during thermobaric instability. *J. Phys. Oceanogr.* 35(8):1359–69
Journaux B, Kalousová K, Sotin C, Tobie G, Vance SD, et al. 2020. High-pressure ices in large ocean worlds. *Space Sci. Rev.* 216(1):7

Kalousová K, Soderlund KM, Solomonidou A, Sotin C. 2024. Structure and evolution of Ganymede's hydrosphere. In *Ganymede*, ed. M Volwerk, MA McGrath, X Jia, T Spohn. Cambridge, UK: Cambridge Univ. Press. In press

Kalousová K, Sotin C. 2020. The insulating effect of methane clathrate crust on Titan's thermal evolution. *Geophys. Res. Lett.* 47(13):e2020GL087481

Kang W, Jansen M. 2022. On icy ocean worlds, size controls ice shell geometry. *Astrophys. J.* 935(2):103

Kang W, Marshall J, Mittal T, Bire S. 2022a. Ocean dynamics and tracer transport over the south pole geysers of Enceladus. *Mon. Not. R. Astron. Soc.* 517(3):3485–94

Kang W, Mittal T, Bire S, Campin JM, Marshall J. 2022b. How does salinity shape ocean circulation and ice geometry on Enceladus and other icy satellites? *Sci. Adv.* 8(29):eabm4665

Kerswell R. 1993. The instability of precessing flow. *Geophys. Astrophys. Fluid Dyn.* 72(1–4):107–44

Khurana KK, Kivelson MG, Stevenson DJ, Schubert G, Russell CT, et al. 1998. Induced magnetic fields as evidence for subsurface oceans in Europa and Callisto. *Nature* 395(6704):777–80

Kivelson MG, Khurana KK, Russell CT, Volwerk M, Walker RJ, Zimmer C. 2000. Galileo magnetometer measurements: a stronger case for a subsurface ocean at Europa. *Science* 289(5483):1340–43

Kivelson MG, Khurana KK, Volwerk M. 2002. The permanent and inductive magnetic moments of Ganymede. *Icarus* 157(2):507–22

Koch I, Fitzsimons S, Samyn D, Tison JL. 2015. Marine ice recycling at the southern McMurdo Ice Shelf, Antarctica. *J. Glaciol.* 61(228):689–701

Koch S, Harlander U, Egbers C, Hollerbach R. 2013. Inertial waves in a spherical shell induced by librations of the inner sphere: experimental and numerical results. *Fluid Dyn. Res.* 45(3):035504

Kvorka J, Čadek O, Tobie G, Choblet G. 2018. Does Titan's long-wavelength topography contain information about subsurface ocean dynamics? *Icarus* 310:149–64

Kvorka J, Čadek O. 2022. A numerical model of convective heat transfer in Titan's subsurface ocean. *Icarus* 376:114853

Lacaze L, Le Gal P, Le Dizès S. 2005. Elliptical instability of the flow in a rotating shell. *Phys. Earth Planet. Inter.* 151(3–4):194–205

Landeau M, Fournier A, Nataf HC, Cébron D, Schaeffer N. 2022. Sustaining Earth's magnetic dynamo. *Nat. Rev. Earth Environ.* 3(4):255–69

Lawrence JD. 2022. *Antarctic ice shelves as ocean world analogs*. PhD Thesis, Ga. Inst. Technol., Atlanta

Lawrence JD, Washam PM, Stevens C, Hulbe C, Horgan HJ, et al. 2023. Crevasse refreezing and signatures of retreat observed at Kamb Ice Stream grounding zone. *Nat. Geosci.* 16:238–43

Le Bars M, Cébron D, Le Gal P. 2015. Flows driven by libration, precession, and tides. *Annu. Rev. Fluid Mech.* 47:163–93

Le Reun T, Favier B, Barker AJ, Le Bars M. 2017. Inertial wave turbulence driven by elliptical instability. *Phys. Rev. Lett.* 119(3):034502

Le Reun T, Favier B, Le Bars M. 2018. Parametric instability and wave turbulence driven by tidal excitation of internal waves. *J. Fluid Mech.* 840:498–529

Le Reun T, Favier B, Le Bars M. 2019. Experimental study of the nonlinear saturation of the elliptical instability: inertial wave turbulence versus geostrophic turbulence. *J. Fluid Mech.* 879:296–326

LeBlond PH, Mysak LA. 1978. *Waves in the Ocean*. Amsterdam: Elsevier

Lemasquerier D, Bierson CJ, Soderlund KM. 2022. *Can convection in icy moons' oceans translate interior tidal heating patterns to the ice-ocean boundary?* Paper presented at the American Geophysical Society Fall Meeting, Chicago, Dec. 12–16

Lemasquerier D, Grannan A, Vidal J, Cébron D, Favier B, et al. 2017. Libration-driven flows in ellipsoidal shells. *J. Geophys. Res. Planets* 122(9):1926–50

Lewis EL, Perkin RG. 1986. Ice pumps and their rates. *J. Geophys. Res.* 91:11756–62

Lin Y, Marti P, Noir J. 2015. Shear-driven parametric instability in a precessing sphere. *Phys. Fluids* 27(4):046601

Lobo AH, Thompson AF, Vance SD, Tharimena S. 2021. A pole-to-equator ocean overturning circulation on Enceladus. *Nat. Geosci.* 14(4):185–89

Lowell RP, DuBose M. 2005. Hydrothermal systems on Europa. *Geophys. Res. Lett.* 32:L05202

Maas LRM. 2005. Wave attractors: linear yet nonlinear. *Int. J. Bifurc. Chaos* 15(9):2757–82
Malkus W. 1968. Precession of the earth as the cause of geomagnetism: Experiments lend support to the proposal that precessional torques drive the earth's dynamo. *Science* 160(3825):259–64
Matsuyama I. 2014. Tidal dissipation in the oceans of icy satellites. *Icarus* 242:11–18
Matsuyama I, Beuthe M, Hay HC, Nimmo F, Kamata S. 2018. Ocean tidal heating in icy satellites with solid shells. *Icarus* 312:208–30
McKinnon WB. 1984. On the origin of Triton and Pluto. *Nature* 311(5984):355–58
Melosh HJ, Ekholm AG, Showman AP, Lorenz RD. 2004. The temperature of Europa's subsurface water ocean. *Icarus* 168:498–502
Morize C, Le Bars M, Le Gal P, Tilgner A. 2010. Experimental determination of zonal winds driven by tides. *Phys. Rev. Lett.* 104(21):214501
Natl. Acad. Sci. 2022. *Origins, Worlds, and Life: A Decadal Strategy for Planetary Science and Astrobiology 2023–2032*. Washington, DC: Natl. Acad. Press
Neveu M, Rhoden AR. 2019. Evolution of Saturn's mid-sized moons. *Nat. Astron.* 3(6):543–52
Nimmo F, Pappalardo RT. 2016. Ocean worlds in the outer solar system. *J. Geophys. Res. Planets* 121(8):1378–99
Nimmo F, Spencer J. 2015. Powering Triton's recent geological activity by obliquity tides: implications for Pluto geology. *Icarus* 246:2–10
Nobili C, Meunier P, Favier B, Le Bars M. 2021. Hysteresis and instabilities in a spheroid in precession near the resonance with the tilt-over mode. *J. Fluid Mech.* 909:A17
Noir J, Cébron D, Le Bars M, Sauret A, Aurnou J. 2012. Experimental study of libration-driven zonal flows in non-axisymmetric containers. *Phys. Earth Planet. Inter.* 204–5:1–10
Noir J, Hemmerlin F, Wicht J, Baca S, Aurnou J. 2009. An experimental and numerical study of librationally driven flow in planetary cores and subsurface oceans. *Phys. Earth Planet. Inter.* 173(1–2):141–52
Ojakangas GW, Stevenson DJ. 1989. Thermal state of an ice shell on Europa. *Icarus* 81(2):220–41
Pappalardo RT, Belton MJS, Breneman HH, Carr MH, Chapman CR, et al. 1999. Does Europa have a subsurface ocean? Evaluation of the geological evidence. *J. Geophys. Res. Planets* 104(E10):24015–55
Peale SJ. 1999. Origin and evolution of the natural satellites. *Annu. Rev. Astron. Astrophys.* 37:533–602
Peterson G, Nimmo F, Schenk P. 2015. Elastic thickness and heat flux estimates for the Uranian satellite Ariel. *Icarus* 250:116–22
Porco CC, Helfenstein P, Thomas PC, Ingersoll AP, Wisdom J, et al. 2006. Cassini observes the active south pole of Enceladus. *Science* 311(5766):1393–401
Rekier J, Trinh A, Triana SA, Dehant V. 2019. Internal energy dissipation in Enceladus's subsurface ocean from tides and libration and the role of inertial waves. *J. Geophys. Res. Planets* 124(8):2198–212
Renaud JP, Henning WG, Saxena P, Neveu M, Bagheri A, et al. 2021. Tidal dissipation in dual-body, highly eccentric, and nonsynchronously rotating systems: applications to Pluto-Charon and the exoplanet TRAPPIST-1e. *Planet. Sci. J.* 2(1):4
Rhoden AR, Walker ME. 2022. The case for an ocean-bearing Mimas from tidal heating analysis. *Icarus* 376:114872
Richard A, Rambaux N, Charnay B. 2014. Librational response of a deformed 3-layer Titan perturbed by non-Keplerian orbit and atmospheric couplings. *Planet. Space Sci.* 93:22–34
Rieutord M, Georgeot B, Valdettaro L. 2001. Inertial waves in a rotating spherical shell: attractors and asymptotic spectrum. *J. Fluid Mech.* 435:103–44
Robinson NJ, Williams MJM, Stevens CL, Langhorne PJ, Haskell TG. 2014. Evolution of a supercooled ice shelf water plume with an actively growing subice platelet matrix. *J. Geophys. Res. Oceans* 119(6):3425–46
Ross MN, Schubert G. 1990. The coupled orbital and thermal evolution of Triton. *Geophys. Res. Lett.* 17(10):1749–52
Rovira-Navarro M, Matsuyama I, Hay HCFC. 2023. Thin-shell tidal dynamics of ocean worlds. *Planet. Sci. J.* 4(2):23
Rovira-Navarro M, Rieutord M, Gerkema T, Maas LR, van der Wal W, Vermeersen B. 2019. Do tidally-generated inertial waves heat the subsurface oceans of Europa and Enceladus? *Icarus* 321:126–40
Sasaki T, Stewart GR, Ida S. 2010. Origin of the different architectures of the Jovian and Saturnian satellite systems. *Astrophys. J.* 714(2):1052–64

Saur J, Duling S, Roth L, Jia X, Strobel DF, et al. 2015. The search for a subsurface ocean in Ganymede with Hubble Space Telescope observations of its auroral ovals. *J. Geophys. Res. Space Phys.* 120(3):1715–37
Sauret A, Cébron D, Le Bars M. 2013. Spontaneous generation of inertial waves from boundary turbulence in a librating sphere. *J. Fluid Mech.* 728:R5
Sauret A, Cébron D, Morize C, Le Bars M. 2010. Experimental and numerical study of mean zonal flows generated by librations of a rotating spherical cavity. *J. Fluid Mech.* 662:260–68
Sauret A, Le Bars M, Le Gal P. 2014. Tide-driven shear instability in planetary liquid cores. *Geophys. Res. Lett.* 41(17):6078–83
Schenk P. 2010. *Atlas of the Galilean Satellites*. Cambridge, UK: Cambridge Univ. Press
Schmidt BE, Washam P, Davis PED, Nicholls KW, Holland DM, et al. 2023. Heterogeneous melting near the Thwaites Glacier grounding line. *Nature* 614(7948):471–78
Schoenfeld AM, Hawkins EK, Soderlund KM, Vance SD, Leonard E, Yin A. 2023. Particle entrainment and rotating convection in Enceladus' ocean. *Commun. Earth Environ.* 4(1):28
Smith BA, Soderblom LA, Banfield D, Barnet C, Basilevsky AT, et al. 1989. Voyager 2 at Neptune: imaging science results. *Science* 246(4936):1422–49
Smith BA, Soderblom LA, Beebe R, Bliss D, Boyce JM, et al. 1986. Voyager 2 in the Uranian system: imaging science results. *Science* 233(4759):43–64
Soderlund KM. 2019. Ocean dynamics of outer solar system satellites. *Geophys. Res. Lett.* 46(15):8700–10
Soderlund KM, Kalousová K, Buffo JJ, Glein CR, Goodman JC, et al. 2020. Ice-ocean exchange processes in the Jovian and Saturnian satellites. *Space Sci. Rev.* 216(5):80
Soderlund KM, Schmidt BE, Wicht J, Blankenship DD. 2014. Ocean-driven heating of Europa's icy shell at low latitudes. *Nat. Geosci.* 7:16–19
Sotin C, Kalousová K, Tobie G. 2021. Titan's interior structure and dynamics after the Cassini-Huygens mission. *Annu. Rev. Earth Planet. Sci.* 49:579–607
Staquet C, Sommeria J. 2002. Internal gravity waves: from instabilities to turbulence. *Annu. Rev. Fluid Dyn.* 34:559–93
Stewartson K. 1966. On almost rigid rotations. Part 2. *J. Fluid Mech.* 26(1):131–44
Stewartson K, Rickard JA. 1969. Pathological oscillations of a rotating fluid. *J. Fluid Mech.* 35(4):759–73
Straneo F, Cedenese C. 2015. The dynamics of Greenland's glacial fjords and their role in climate. *Annu. Rev. Mar. Sci.* 7:89–112
Terra-Nova F, Amit H, Choblet G, Tobie G, Bouffard M, Čadek O. 2023. The influence of heterogeneous seafloor heat flux on the cooling patterns of Ganymede's and Titan's subsurface oceans. *Icarus* 389:115232
Thomson RE, Delaney JR. 2001. Evidence for a weakly stratified Europan ocean sustained by seafloor heat flux. *J. Geophys. Res.* 106:12355–65
Tilgner A. 2007. Zonal wind driven by inertial modes. *Phys. Rev. Lett.* 99(19):194501
Townsend AA. 1964. Natural convection in water over an ice surface. *Q. J. R. Meteorol. Soc.* 90(385):248–59
Tritton DJ. 1998. *Physical Fluid Dynamics*. Oxford, UK: Oxford Univ. Press
Tyler RH. 2008. Strong ocean tidal flow and heating on moons of the outer planets. *Nature* 456(7223):770–72
Tyler RH. 2011a. Magnetic remote sensing of Europa's ocean tides. *Icarus* 211:906–8
Tyler RH. 2011b. Tidal dynamical considerations constrain the state of an ocean on Enceladus. *Icarus* 211(1):770–79
Tyler RH. 2014. Comparative estimates of the heat generated by ocean tides on icy satellites in the outer Solar System. *Icarus* 243(Suppl. C):358–85
Van Hoolst T, Rambaux N, Karatekin Ö, Dehant V, Rivoldini A. 2008. The librations, shape, and icy shell of Europa. *Icarus* 195(1):386–99
Vance SD, Goodman JC. 2009. Oceanography of an ice-covered moon. In *Europa*, ed. RT Pappalardo, WB McKinnon, KK Khurana, pp. 459–82. Tucson: Univ. Ariz. Press
Vance SD, Panning MP, Stahler S, Cammarano F, Bills BG, et al. 2018. Geophysical investigations of habitability in ice-covered ocean worlds. *J. Geophys. Res.* 123:180–205
Vance SD, Styczinski MJ, Bills BG, Cochrane CJ, Soderlund KM, et al. 2020. Magnetic induction responses of Jupiter's ocean moons including effects from adiabatic convection. *J. Geophys. Res. Planets* 126(2):e2020JE006418

Vilella K, Choblet G, Tsao WE, Deschamps F. 2020. Tidally heated convection and the occurrence of melting in icy satellites: application to Europa. *J. Geophys. Res. Planets* 125(3):e2019JE006248
Waite JH, Glein CR, Perryman RS, Teolis BD, Magee BA, et al. 2017. Cassini finds molecular hydrogen in the Enceladus plume: evidence for hydrothermal processes. *Science* 356:155–59
Walker ME, Rhoden AR. 2022. Tidal heating at Europa using the Multifrequency Analysis of Tidal Heating toolkit. *Planet. Sci. J.* 3(7):149
Washam P, Münchow A, Nicholls KW. 2018. A decade of ocean changes impacting the ice shelf of Petermann Gletscher, Greenland. *J. Phys. Oceanogr.* 48(10):2477–93
Wilson A, Kerswell RR. 2018. Can libration maintain Enceladus's ocean? *Earth Planet. Sci. Lett.* 500:41–46
Wolfenbarger NS, Buffo JJ, Soderlund KM, Blankenship DD. 2022. Ice shell structure and composition of ocean worlds: insights from accreted ice on Earth. *Astrobiology* 22(8):937–61
Wong T, Hansen U, Wiesehöfer T, McKinnon WB. 2022. Layering by double-diffusive convection in the subsurface oceans of Europa and Enceladus. *J. Geophys. Res. Planets* 127(12):e2022JE007316
Wunsch C, Ferrari R. 2004. Vertical mixing, energy, and the general circulation of the oceans. *Annu. Rev. Fluid Mech.* 36:281–314
Xie X, Liu X, Chen Z, Wang Y, Chen D, et al. 2023. Pure inertial waves radiating from low-frequency flows over large-scale topography. *Geophys. Res. Lett.* 50(4):e2022GL099889
Zannoni M, Hemingway D, Gomez Casajus L, Tortora P. 2020. The gravity field and interior structure of Dione. *Icarus* 345:113713
Zeng Y, Jansen MF. 2021. Ocean circulation on Enceladus with a high-versus low-salinity ocean. *Planet. Sci. J.* 2(4):151
Zhang K, Chan KH, Liao X, Aurnou JM. 2013. The non-resonant response of fluid in a rapidly rotating sphere undergoing longitudinal libration. *J. Fluid Mech.* 720:212–35